Materials Today Chemistry 11 (2019) 253–268

Contents lists available at ScienceDirect

Materials Today Chemistry

journal homepage: www.journals.elsevier.com/materials-today-chemistry/

Low-dimensional heteroatom-doped carbon nanomaterials prepared with thermally removable templates for the electrocatalytic reduction of oxygen

Dengke Zhao [a, 1], Xiaojing Zhu [a, 1], Nan Wang [a, 1], Bingzhang Lu [b], Ligui Li [a, **], Shaowei Chen [a, b, *]

[a] Guangzhou Key Laboratory for Surface Chemistry of Energy Materials, New Energy Research Institute, School of Environment and Energy, South China University of Technology, Guangzhou Higher Education Mega Center, Guangzhou 510006, China
[b] Department of Chemistry and Biochemistry, University of California, 1156 High Street, Santa Cruz, CA 95064, USA

ARTICLE INFO

Article history:
Received 21 October 2018
Received in revised form
12 November 2018
Accepted 14 November 2018

Keywords:
Nitrogen-doped carbon
Oxygen reduction reaction
Pyrolysis
Thermally removable template

ABSTRACT

Low-dimensional heteroatom-doped carbon nanomaterials represent a promising low-cost alternative to the conventional noble metal-based catalysts towards oxygen reduction reaction (ORR), a key process at the cathodes of fuel cells and metal-air batteries. It has been found that the electrocatalytic activity depends on the effective surface area and porosity, which dictate the accessibility of the catalytic active sites and mass transfer involved in the reaction. Toward this end, thermally removable templates have been used extensively in the preparation of a range of low-dimensional heteroatom-doped porous carbon nanomaterials that exhibit remarkable electrocatalytic activity towards ORR. In this article, we will summarize recent progress in this area of research and conclude with a perspective of the challenges and opportunities in future research.

1. Introduction

Oxygen reduction reaction (ORR) is a key reaction in a wide range of electrochemical energy storage and conversion technologies [1–3]. For instance, in proton exchange membrane fuel cells, alkaline direct methanol fuel cells and metal-air batteries, small molecule fuels or metals are oxidized at the anode, and concurrently oxygen is reduced at the cathode [4–8]. Yet, the sluggish electron-transfer kinetics of ORR significantly limits the energy conversion efficiency of the electrochemical technologies [9]. In practical applications, a sufficiently high current density is generally required. Thus, high-performance electrocatalysts are needed, and noble metals, in particular, Pt, Pd, and their alloy nanoparticles, are the leading choices because of their high catalytic activity [10,11]. However, the high costs, poor durability, and low poison resistance of these noble metal-based electrocatalysts have severely impeded the widespread commercialization of these electrochemical energy technologies [12,13].

To mitigate these issues, low-dimensional heteroatom-doped carbons represent an emerging family of non-precious metal-based electrocatalysts for ORR, due to various distinct advantages, such as low costs, ready availability of diverse precursors, relative ease of sample synthesis, high chemical stability, good electrical conductivity, and considerable catalytic activity [14–18]. Importantly, the morphologies of the carbon materials can be readily tailored with the aid of structural templates and/or by controlling pyrolytic conditions, and the electronic structure can also be easily tuned by doping with select heteroatoms, such as N, P, B, S, Se, and metal elements such as Fe, Co, and Ni [19–29]. Deliberate manipulation of these structural variables plays a key role in optimizing the performance of the ORR electrocatalysts.

In these studies, identification of the catalytic active sites represents a critical first step; yet, this remains a matter of active debates [12,30]. Nevertheless, it is generally believed that the specific surface area and porous structure of the carbon catalysts significantly influence the accessibility of the active sites and hence the eventual electrocatalytic performance [2,31,32]. Along this line, it is highly desired to maximize the electrochemical surface area, particularly by the formation of mesopores (2–50 nm), so that mass

* Corresponding author.
** Corresponding author.
E-mail addresses: esguili@scut.edu.cn, shaowei@ucsc.edu (S. Chen).
[1] These authors contribute equally to this work.

https://doi.org/10.1016/j.mtchem.2018.11.004
2468-5194/

transfer of related species (e.g., H_2O, OH^-, H^+, O_2, and so forth) can be facilitated, another important factor that impacts the ORR activity [33]. In fact, a number of methods have been developed for the preparation of highly porous carbons, in which direct carbonization/pyrolysis of carbonaceous precursors, such as the intrinsically porous metal–organic frameworks (MOFs), is deemed as an ideal way for the synthesis of carbon nanomaterials with highly controlled pore structures [34,35]. Unfortunately, the thus-synthesized carbons usually show a low surface area, primarily due to the collapse of pores at high temperatures and agglomeration of the carbon skeletons [36].

To mitigate the collapse/agglomeration problem, rigid templates are usually used during carbonization. For instance, SiO_2 nanoparticles, porous anodic alumina, and layered metal hydroxides have been widely used for the preparation of porous carbon-based nanomaterials with a high surface area and remarkable catalytic activity [31,33,37,38]. However, such conventional 'rigid template' strategies inevitably involve multiple time- and energy-consuming procedures, such as postsynthesis removal of excess templates by wet chemical etching, repeated sample purifications, freeze-drying for mitigating the decrease of surface area due to recollapse of pores, and so forth, which complicate the synthesis process and hence impede the scale-up production and cost reduction. What is more, the electrocatalytic activity may be compromised because part of the catalytically active species may be lost in the postsynthesis template removal process by, for instance, harsh acidic/basic etching.

Within this context, thermally removable templates have been attracting extensive interest in recent research. These templates can help prevent the collapse of pores during high-temperature carbonization and be concurrently removed via the formation of volatile species [39,40]. Thus, no postsynthesis template removal is needed. In fact, this strategy has been proven to be effective, versatile, and robust in the preparation of low-dimensional carbon materials for efficient ORR electrocatalysis. In this review, we will summarize recent progress in the synthesis of low-dimensional carbons for ORR based on thermally removable templates, with a focus on structural engineering of the resulting doped carbons and the correlation with the electrocatalytic activity towards ORR in various electrochemical energy systems [41].

2. Thermally removable templates

2.1. Zinc-based compounds

Zinc-based compounds are cost-effective and abundant, and usually show relatively low boiling points, which make them viable candidates as thermally removable templates in the pyrolytic synthesis of porous carbons [42–47]. For instance, Lin et al. [47] recently grew MOFs on commercially available ZnO nanowires (ZnO NWs), which, after pyrolysis at high temperatures, produced one-dimensional (1D) N-doped carbon nanotubes embedded with $Co@CoO_x$ core-shell nanoparticles ($Co@CoO_x$/NCNT) (Fig. 1). In this procedure, ZnO NWs were used as structural templates as well as nucleation sites for the deposition of ZIF-8 crystals, where the ZnO NWs were partially dissolved producing the Zn source needed for the growth of bimetal Zn/Co-ZIF. In the subsequent high-temperature pyrolysis, ZnO NWs were in situ reduced to Zn^0 by a carbothermic reaction with carbon and evaporated due to the relatively low boiling point (ca. 910 °C), leaving behind a tubular morphology. As for the reference samples prepared with Zn/Co-ZIF precursor particles in the absence of ZnO NWs, high-temperature pyrolysis depleted Zn during the early stages of pyrolysis, leading to substantial agglomeration. This agglomeration was markedly diminished by the excess supply of volatile Zn from the ZnO NWs templates, which facilitated the formation of an electrochemically favorable hierarchical porous structure. Moreover, the excess oxygen from ZnO NWs, possibly released in the form of CO_2 and NO_2, reacted with the in-situ–produced metallic cobalt nanoparticles (Co NPs) to generate a cobalt oxide shell, resulting in the formation of $Co@CoO_x$ core-shell structures with an average diameter of ca. 18 nm (Fig. 2a–c). The corresponding $Co@CoO_x$/NCNT samples showed a high ORR activity, where the onset potential (E_{onset} = +0.94 V vs reversible hydrogen electrode (RHE)) and half-wave potential ($E_{1/2}$ = +0.80 V vs RHE) are very close to those of commercial Pt/C catalyst (Fig. 2d), but the kinetic current density at +0.70 V was three times higher (Fig. 2e).

In another study, Wang et al. [48] described a general route to the preparation of hierarchically porous nitrogen-doped carbon nanofibers (HP-NCNFs) through the pyrolysis of $Zn(OAc)_2$-containing polyvinylpyrrolidone (PVP) nanofibers (NFs). ZnO NPs were

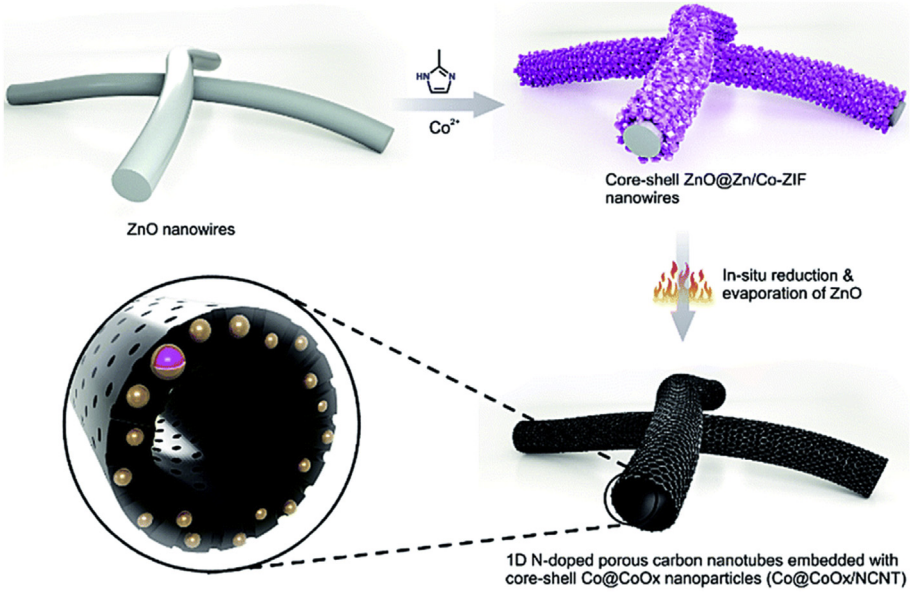

Fig. 1. Schematically illustrating the synthesis process of 1D $Co@CoO_x$/NCNTs. Reprinted with permission from the study by Lin et al. [47]. © 2017, Royal Society of Chemistry.

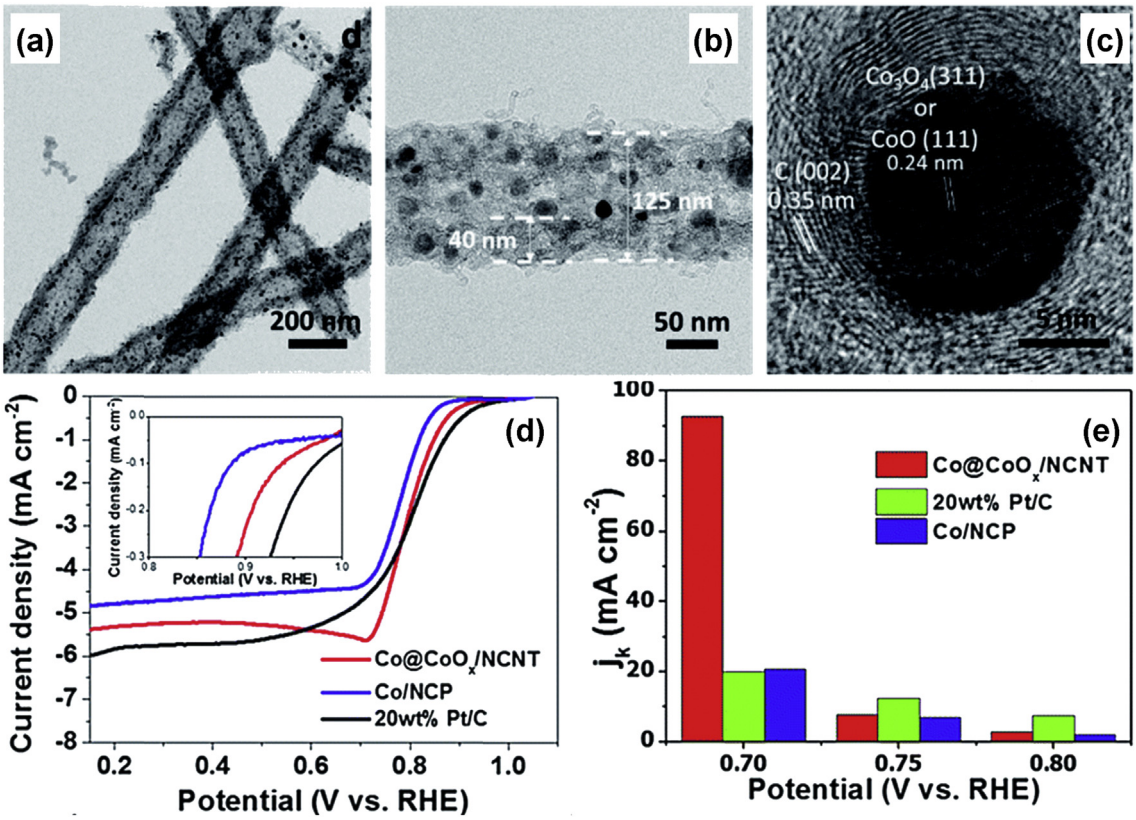

Fig. 2. (a, b) TEM and (c) HR-TEM images of Co@CoO_x/NCNT. (d) ORR polarization curves of 20 wt% Pt/C (black), Co/N-doped carbon nano-polyhedron (NCP) (blue), and Co@CoO_x/NCNT (red) in O_2-saturated electrolyte (scan rate: 10 mV s^{-1}, rotation rate: 1600 rpm). (e) Comparison of J_k at 0.70 V, 0.75 V, and 0.80 V for 20 wt% Pt/C, Co/NCP, and Co@CoOx/NCNT. Adapted with permission from the study by Lin et al. [47]. © 2017, Royal Society of Chemistry.

formed in situ and homogeneously embedded in the fiber precursor and acted as thermally removable templates in pyrolysis. As shown in Fig. 3a, $Zn(OAc)_2$-PVP NFs were prepared by electrospinning the DMF solution containing $Zn(OAc)_2$ and PVP. The as-spun $Zn(OAc)_2$-PVP NFs were preannealed at 200 °C in air to stabilize the structure and also to remove residual DMF. Moreover, this treatment transformed the $Zn(OAc)_2$ into ZnO, while the relatively stable PVP remained unchanged, leading to the formation of ZnO-PVP NFs. Subsequently, the ZnO-PVP NFs were pyrolyzed at 800 °C in a nitrogen atmosphere, which resulted in the reduction of ZnO to Zn by carbon, $ZnO(s) + C(s) \rightarrow Zn(g) + CO(g)$, accompanied by the generation of CO [49]. The produced Zn was then sublimated and escaped from the carbon matrix. During this pyrolysis process, the release of Zn vapors as well as other gases (e.g., CO, CO_2) created a larger number of hierarchical pores than the conventional NCNFs (Fig. 3b–c), affording HP-NCNFs (Fig. 3d–e), leading to a more positive onset potential, a much higher limiting current density (Fig. 3f) as well as significantly higher kinetic current density (Fig. 3g) than the conventional NCNFs, although the onset potential was slightly lower than that of commercial Pt/C catalyst [50–52].

Recently, Li et al. [53] demonstrated a facile strategy to prepare atom-thin carbon nanomesh clusters (CMCs) through a sacrificial and morphology-preserved thermal transformation of electrodeposited zinc-coordinated polymer (Zn-CP). The synthesis procedure is schematically illustrated in Fig. 4a. First, Zn-CP clusters were in situ formed on a Zn foil by electrodeposition in the aqueous solution of 0.1 M Na_2SO_4 and 1 M Hmim (Hmim = 2-methylimidazole) at an applied potential of 6 V for a duration of 2 min. The Zn foil served as both a sacrificial metal source and a substrate for electrodeposition. At potentials higher than +0.7 V [54], Zn was oxidized to Zn^{2+} which then reacted with Hmim and SO_4^{2-} linkers. After electrodeposition, Zn-CP clusters were scrapped from the Zn foil and calcined at 900 °C in an Ar/H_2 mixture flow to form CMC. The thus-obtained CMC was further doped with nitrogen by annealing in the presence of melamine, affording nitrogen-doped CMC (N-CMC). Scanning electron microscopy (SEM) and transmission electron microscopy (TEM) studies (Fig. 4b–f) showed a 3D-cluster morphology of the N-CMC that comprised rippled and wrinkled plates. The thickness of the assembled plates after annealing was found to decrease because of the volatilization of Zn and gaseous products [55]. The TEM images at higher magnifications of the N-CMC plates (Fig. 4g and h) confirmed the formation of a large number of hierarchically arranged pores with the diameter ranging from a few to tens of nanometers. The formation of mesh-like carbon clusters with a high density of nanopores was attributed to thermal annealing, where the H_2 atmosphere impacted the formation of carbon nanomesh structure, whereas the Zn^{2+} cations were reduced by H_2 in the Ar/H_2 mixture flow to metallic Zn^0. In addition, as the annealing was conducted at 900 °C that was close to the boiling point of bulk zinc, the in situ–formed metallic Zn^0 was vaporized and released, facilitating the formation of a high density of hierarchical pores in the N-CMC cluster plates [56]. In addition, the release of gaseous SO_3, H_2O and other small organic molecules resulting from the pyrolysis of Zn-CP might also contribute to the formation of nanopores in N-CMC. In electrochemical tests, linear sweep voltammetric (LSV) measurements conducted in a 0.1 M KOH aqueous solution (Fig. 4i) showed that the N-CMC sample exhibited an ORR activity highly comparable to that of commercial Pt/C catalysts in terms of half-wave potential ($E_{1/2}$ = +0.81 V for N-CMC vs RHE, and +0.83 V for Pt/C) and the diffusion-limited current density

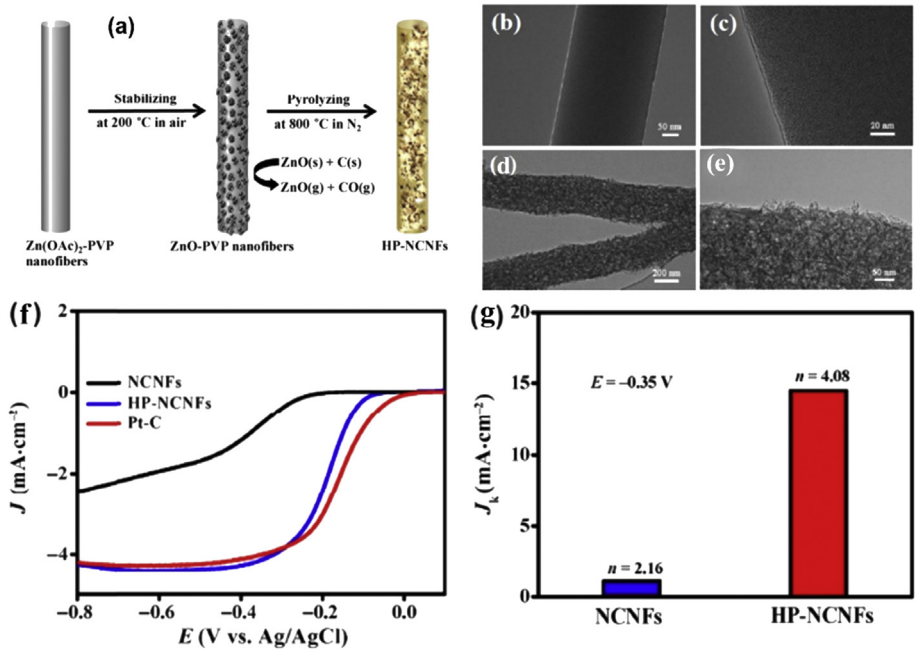

Fig. 3. (a) Schematic illustration of the fabrication process of HP-NCNFs. (b, c) TEM images of NCNFs and (d, e) HP-NCNFs. (f) LSV measurement for Pt/C, NCNFs and HP-NCNFs in O_2-saturated 0.1 M KOH solution at a scan rate of 10 mV s^{-1}. (g) Kinetic-limiting current densities of HP-NCNFs and NCNFs at −0.35 V. Adapted with permission from the study by Wang et al. [48]. © 2016, Springer Nature.

at +0.40 V, signifying the high potential of using Zn-containing compounds as thermally removable templates in the preparation of effective carbon electrocatalysts for ORR.

2.2. Iron-containing compounds

Recently, we showed that Fe-containing compounds could also be used as effective thermally removable templates for the preparation of Fe,N-codoped porous carbons [41]. As depicted in Fig. 5a, 2-fluoroaniline was oxidized by $FeCl_3$ to initiate the polymerization process under hydrothermal control, forming poly(2-fluoroaniline) nanosheets that were homogeneously embedded with a large number of FeO(OH) nanorods due to the hydrolysis of $FeCl_3$. Direct pyrolysis of these poly(2-fluoroaniline) nanosheets yielded Fe,N-codoped carbons with abundant mesopores. During pyrolysis, the in-situ–formed FeO(OH) nanocrystals served as rigid templates to prevent the collapse of the carbon skeletons and concurrently promoted the formation of mesopores in the carbon matrix through the regeneration of $FeCl_3$ that was thermally volatile because of its relatively low boiling point (315 °C). In fact, the diameter of the pores formed in the resulting Fe,N-codoped porous carbons was in the range of 10–60 nm, highly comparable to the dimensions of the FeO(OH) nanorods. The detailed reactions involved in the synthesis of mesoporous Fe,N-codoped carbons through this method were proposed as follows,

$$Fe^{3+} + 3H_2O \rightarrow Fe(OH)_3 + 3H^+ \quad (1)$$

$$Fe(OH)_3 \rightarrow FeO(OH) + H_2O\uparrow \quad (2)$$

$$2FeO(OH) \rightarrow Fe_2O_3 + H_2O\uparrow \quad (3)$$

$$3Fe_2O_3 + 4H_2(CH_4, CO, C) \rightarrow 2Fe_3O_4 + 4H_2O(CO_2, CO)\uparrow \quad (4)$$

$$Fe_3O_4 + 4C \rightarrow 3Fe + 4CO\uparrow \quad (5)$$

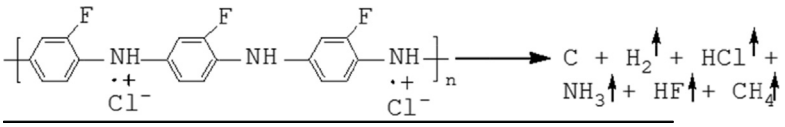

(6)

$$Fe_2O_3 + 6HCL \rightarrow 2FeCl_3\uparrow + 3H_2O\uparrow \quad (7)$$

Specifically, in the aqueous solution of $FeCl_3$ and 2-fluoroaniline, $FeCl_3$ was hydrolyzed to amorphous $Fe(OH)_3$ sol which was promoted by the presence of alkaline 2-fluoroaniline (Eq. (1)), while 2-fluoroaniline was protonated by hydrochloric acid that was generated by $FeCl_3$ hydrolysis and subsequently polymerized into poly(2-fluoroaniline) sheets doped with HCl under hydrothermal conditions, and the amorphous $Fe(OH)_3$ sol was concurrently converted into FeO(OH) nanorods (Eq. (2)) that were homogeneously distributed within the polymer matrix. When the poly(2-fluoroaniline) nanosheets were pyrolyzed at elevated temperatures (600–900 °C), the FeO(OH) nanorods were further converted into Fe_2O_3 crystals (Eq. (3)), and the polymers of low molecular weights were decomposed into multimers and hence sublimated.

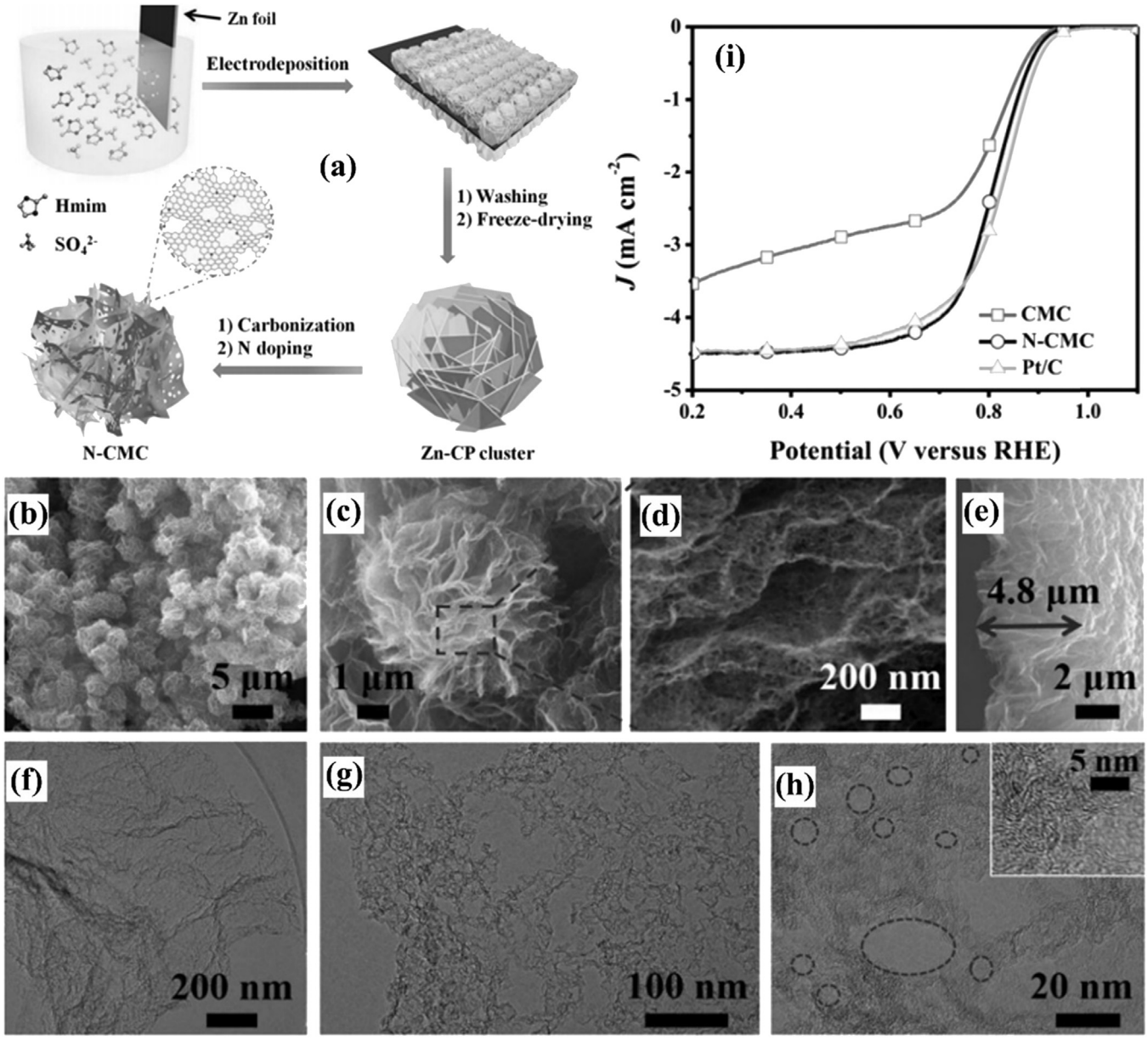

Fig. 4. (a) Schematic illustration of the synthetic procedure of N-CMC. (b, c, and d) SEM images of N-CMC with different magnifications. (e) Cross-sectional SEM image of the assembled microplate. (f, g, and h) TEM image of N-CMC nanosheets. (i) LSV measurements for Pt/C, CMC, and N-CMC in O_2-saturated 0.1 M KOH solution at a scan rate of 10 mV s^{-1}. Adapted with permission from the study by Li et al. [53]. © 2017, Wiley-VCH Verlag GmbH & Co. KGaA.

At higher pyrolysis temperatures (>700 °C), most polymers were carbonized, accompanied by the release of a series of volatile species, such as CO_2, CO, CH_4, HCl, HF, H_2, H_2O, and NH_3 (Eq. (4–6)). Notably, HCl could react with the Fe_2O_3 nanocrystals to form thermally volatile $FeCl_3$ (Eq (7)), in situ generating abundant cavities in the resulting carbon matrix.

The thus-synthesized mesoporous N-doped carbon-based catalysts comprised a trace amount of iron and the sample prepared at 800 °C (Fe-N/C-800) displayed a high specific surface area of 934.8 m^2 g^{-1} and a markedly higher onset potential (+0.980 V vs RHE), larger diffusion-limiting current density, and much higher selectivity towards the four-electron reduction of oxygen (e.g., number of electron transfer n = 3.95 at +0.750 V) than commercial Pt/C catalyst in alkaline electrolytes (Fig. 5b–d). These results highlight the significance of FeO(OH) nanocrystals as thermally removable templates in the synthesis of low dimensional Fe,N-codoped porous carbon electrocatalysts for ORR.

To further enhance the ORR performance of the obtained mesoporous doped carbons, one effective strategy is to incorporate reduced graphene oxide (rGO) nanosheets into the porous carbon catalysts, partly because the electrical conductivity can be markedly enhanced [57–60]. In a subsequent study [57], composite precursors with a sandwich-like polymer/graphene oxide/polymer structure were firstly synthesized in the presence of $FeCl_3$ by the aforementioned hydrothermal polymerization of 2-fluroaniline on the surface of GO sheets (Fig. 6a). Interestingly, in the absence of GO sheets, amorphous Fe-containing species were found to be homogeneously embedded in the resulting poly(2-fluroaniline) rather than in the FeO(OH) nanorods. In the subsequent pyrolysis process, the amorphous Fe-containing species in the polymer matrix was

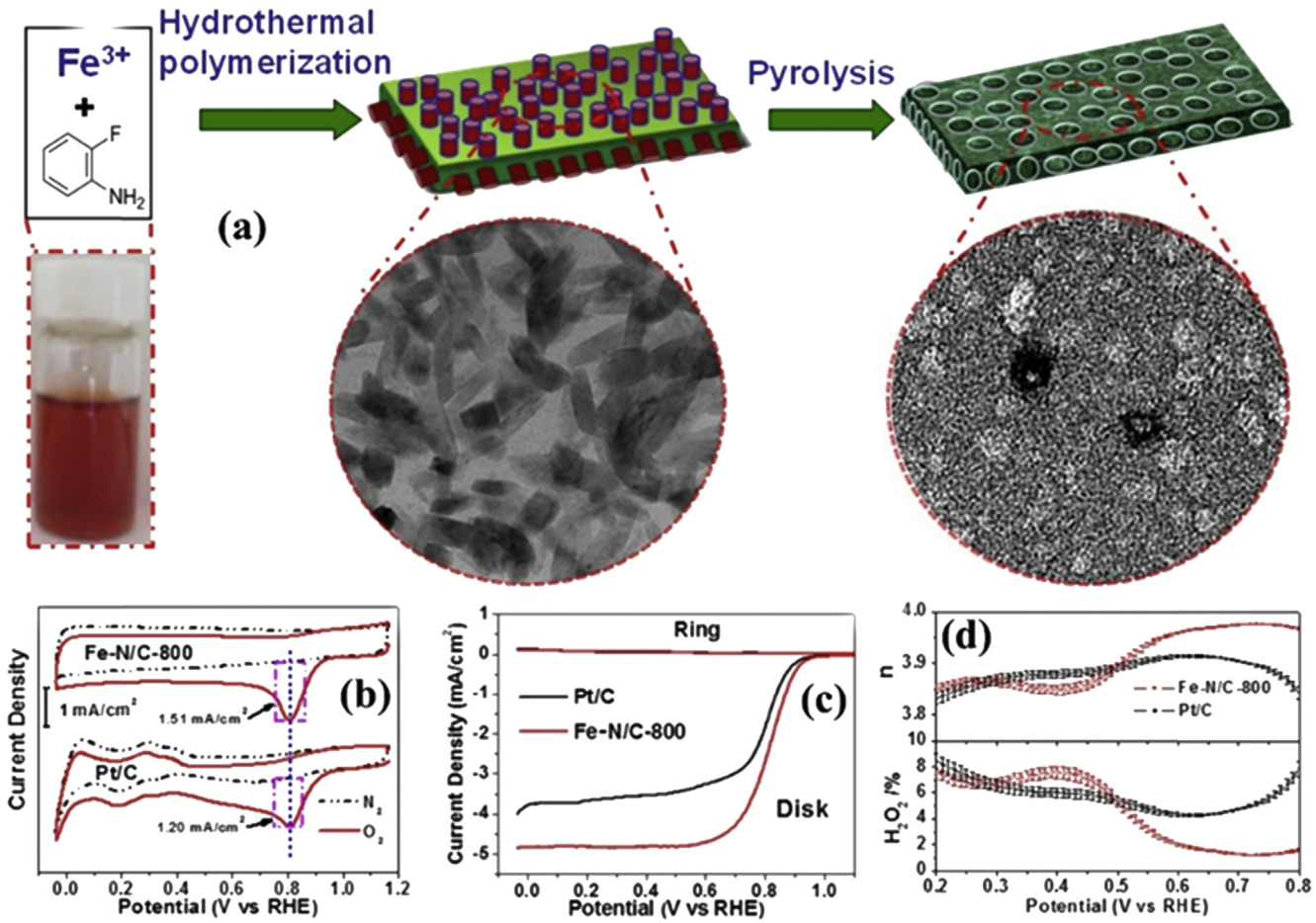

Fig. 5. Schematically illustrating the preparation of N-doped mesoporous carbon catalyst (Fe-N/C) with thermally removable nanoparticles. (b) Cyclic and (c) rotating ring-disk electrode (RRDE) voltammograms, (d) plots of H_2O_2 yield and number of electron transfer of a glassy carbon electrode modified with Fe-N/C-800 and Pt/C catalysts at the rotation speed of 1600 rpm. Reprinted with permission from the study by Niu et al. [41]. ©2015, American Chemical Society.

converted into nanoparticles which eventually became volatile $FeCl_x$ and hence were removed from the carbonized matrix, leading to the formation of porous N-doped carbons on rGO surface (N-MC/rGO) composites (Fig. 6b–c). Such a composite also contained rich nitrogen self-doped active sites and large specific surface areas, leading to a remarkable ORR activity (Fig. 6d) and markedly enhanced durability in alkaline electrolytes, as compared with the Fe/N-C sample (Fig. 6e) prepared without the addition of GO sheets.

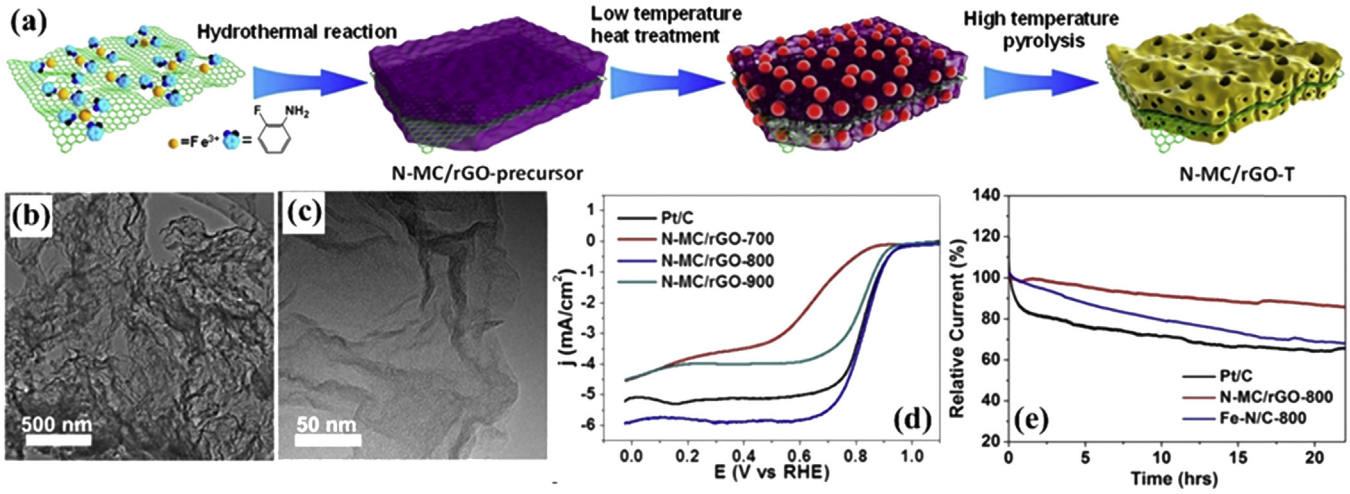

Fig. 6. (a) Schematic illustration of the preparation process of N-MC/rGO-T catalysts by the thermally removable template method. (b, c) TEM images of N-MC/rGO-800. (d) Rotating disk electrode voltammograms. (e) Chronoamperometric curves of Pt/C, Fe-N/C-800, and N-MC/rGO at +0.70 V vs. RHE. Reprinted with permission from the study by Niu et al. [57]. ©2016, Wiley-VCH Verlag GmbH & Co. KGaA.

The remarkable ORR performance of the N-MC/rGO catalyst was ascribed to the synergistic effect between rGO sheets and the N-doped porous carbon layer: (i) the formation of a porous carbon layer on the surface of rGO could effectively impede the restacking of rGO sheets, and maximized the accessibility of ORR active sites; (ii) the high level of graphitization of rGO might provide 2D pathways for electrons and acted as an anticorrosion coating layer for the supported porous carbons [61–63].

In the aforementioned strategy of using Fe-based compounds as thermally removable templates for the preparation of low-dimensional porous carbon-based electrocatalysts, a key step is to form 2D polymer precursors embedded evenly with a high density of thermally volatile nanoscale templates. This is non-trivial, as the loading of nanoscale templates in 0D and 1D polymer precursors is usually rather limited. In addition, hydrothermal polymerization is generally required to prepare the polymer precursors, which is usually conducted in reaction vessels that have a very limited volume and can withstand high temperatures as well as high pressures, impeding the scale-up production. Therefore, it is highly desired to develop more facile routes to the preparation of porous carbon-based ORR electrocatalysts that do not entail the solvothermal or hydrothermal process and are viable for mass production.

More recently, we developed an effective route to ready, scalable preparation of N-doped honeycomb-like porous carbons (HPC), which exhibited a large number of hierarchical macropores and mesopores via simple pyrolysis of sheet-like polypyrrole (PPy) that were synthesized by interface-confined polymerization of pyrrole monomers on NaCl crystal surfaces using $FeCl_3$ as the polymerization initiator (Fig. 7) [64]. Similarly, $FeCl_3$ and derivatives were found to be homogeneously distributed in the resulting PPy sheets and converted into thermally removable nanocrystals in the subsequent pyrolysis process (Fig. 8a–c), which not only promoted the formation of abundant hierarchical pores in the carbonized matrix but also helped generate a high content of nitrogen-containing active sites in the carbon skeletons, leading to the formation of a honeycomb-like highly porous carbon (Fig. 8e), with a specific surface area of 796.8 $m^2\ g^{-1}$ and a high content of nitrogen dopants of 7–18 at.%. Such a morphology was found to facilitate the mass transfer of ORR species and maximize the accessibility of active sites. Indeed, a remarkable ORR activity was observed for the series of HPC catalysts in alkaline electrolytes (Fig. 8d), and the one prepared by pyrolysis at 800 °C outperformed others in the series, with a half-wave potential that was 40 mV more positive than that of the Pt/C benchmark catalysts, along with substantially higher kinetic current density, an electron-transfer number over 3.95 at low overpotentials, improved stability and tolerance to fuel crossover and resistance against CO poisoning. Moreover, when this honeycomb-like N-doped porous carbon was used as an air-diffusion cathode in the assembly of a Zn–air battery (Fig. 8e), its performance was found to surpass commercial Pt/C catalyst (Fig. 8f), demonstrating a high capacity of 647 mA h g^{-1} at a discharged current density of 10 mA cm^{-2} (Fig. 8g) and 617 mA h g^{-1} at 100 mA cm^{-2} as well as a negligible voltage degradation even after continuous operation for 110 h via refueling (Fig. 8h).

2.3. SiO_2 nanoparticle–based thermally removable templates

Pei et al. [65] developed a different route by using SiO_2 nanoparticles as thermally removable templates to prepare N,S-codoped hierarchically porous carbons for oxygen electrocatalysis. The synthesis process is schematically illustrated in Fig. 9a. First, the carbonaceous source, sucrose, was mixed with silica nanospheres and trithiocyanuric acid (TA) to form a homogeneous precursor, into which Teflon powders (5 μm) were then added. In the subsequent pyrolysis at elevated temperatures, the Teflon powders were decomposed into tetrafluoroethylene that reacted with H_2O released from the polymerization and carbonization of sucrose to form HF, and hence, the embedded SiO_2 nanospheres were etched

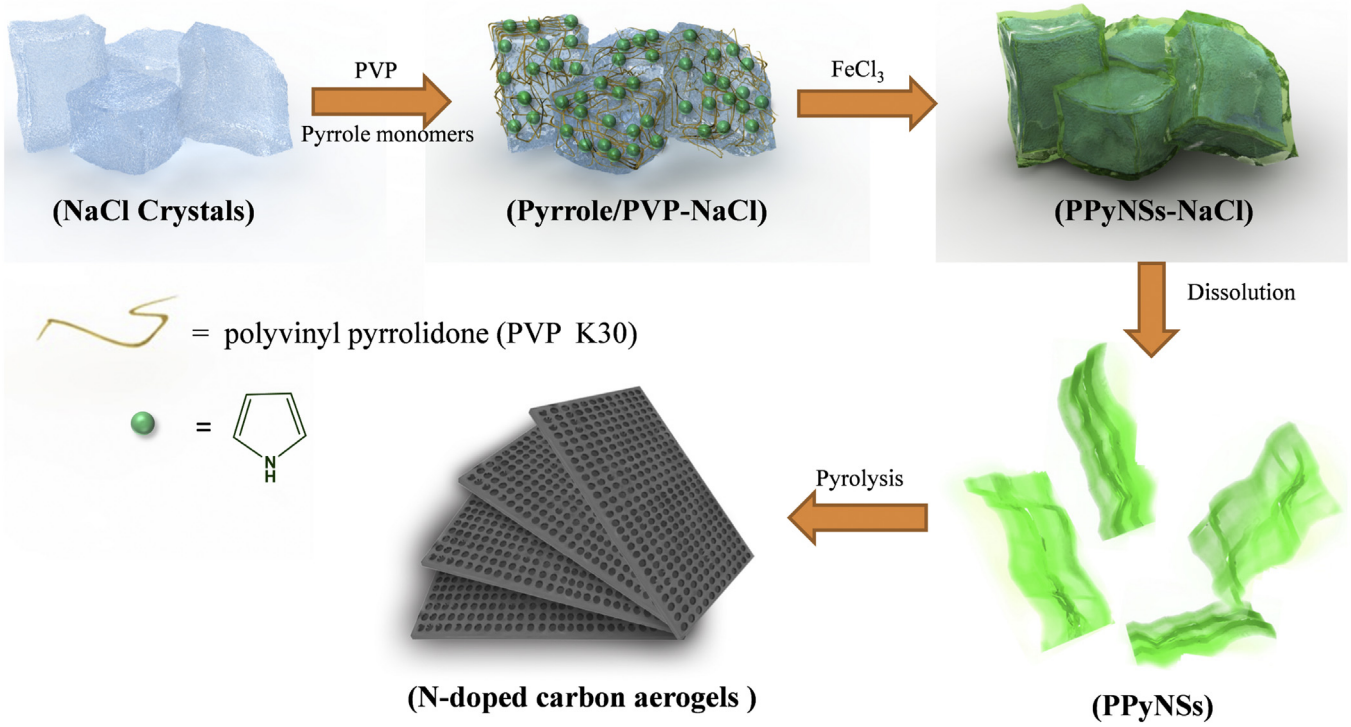

Fig. 7. Schematic illustration of the preparation of nitrogen-doped honeycomb-like porous carbons. Reproduced with permission from the study by Niu et al. [64]. ©2016, Royal Society of Chemistry.

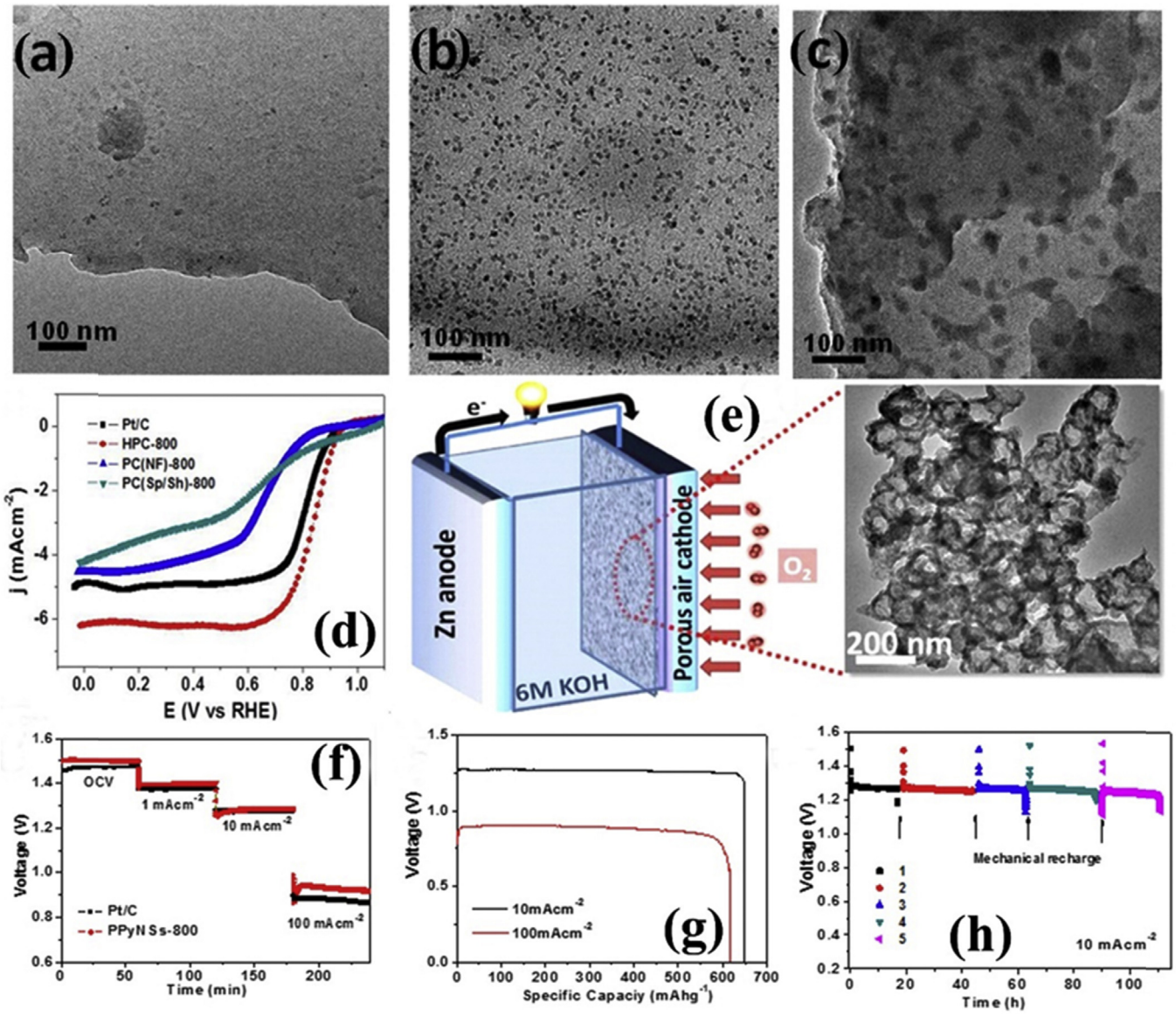

Fig. 8. TEM images showing the evolution of Fe-containing species in polypyrrole nanosheets prepared at (a) room temperature, (b) 300 °C, (c) 500 °C. (d) Rotating disk electrode (RDE) voltammograms of HPC-800, PC(NF)-800, PC(Sp/Sh)-800 and 0.2 mg cm^{-2} of Pt/C in O_2-saturated 0.1 M KOH solution at a rotation speed of 1600 rpm. (e) A sketch showing the structure of a Zn-air battery and the TEM image of HPC-800. (f) Typical galvanostatic discharge curves of a Zn–air battery with HPC-800 and Pt/C as air-diffusion cathode at various current densities (1, 10, and 100 mA cm^{-2}), (g) Long-time galvanostatic discharge curves of a Zn-air battery using HPC-800 as the air-diffusion cathode. (h) 'Recharging' the Zn-air battery using HPC-800 as the cathode catalyst by refilling the Zn anode and electrolyte. The catalyst loading in air cathode was 2.0 mg cm^{-2} for HPC-800 and 1.0 mg cm^{-2} for Pt/C, and the electrolyte for Zn-air cell measurements was 6.0 M KOH. Reproduced with permission from the study by Niu et al. [64]. ©2016, Royal Society of Chemistry.

to form thermally volatile SiF_4 [66,67]. The corresponding processes are proposed as follows (Eqs. (8)–(12)),

$$n C_{12}H_{22}O_{11} \longrightarrow \left[C_{12}H_{20}O_{10}\right]_n + n H_2O \quad (8)$$

$$\left[C_{12}H_{20}O_{10}\right]_n \longrightarrow 12n\,C + 10n H_2O \quad (9)$$

$$\left[C_2F_4\right]_n \longrightarrow n\,C_2F_4\uparrow \quad (10)$$

$$C_2F_4 + 2H_2O \rightarrow 2\,CO\uparrow + 4HF\uparrow \quad (11)$$

$$SiO_2 + 4HF \rightarrow SiF_4\uparrow + 2H_2O \quad (12)$$

As TA has a high content of N and S and is easy to completely decompose at high temperatures, it can serve not only as a good source of sulfur and nitrogen in doping the resulting carbons but also as a good foaming reagent in pore formation. Indeed the resulting N,S-codoped carbon was found to be highly graphitized and comprise abundant cavities of diverse sizes (Fig. 9b), indicative of the formation of hierarchical porous structures. In this procedure, the rigid silica nanospheres helped prevent the collapse of carbonaceous matrix at the early stage of pyrolysis and were subsequently volatilized to promote the formation of abundant hierarchical pores within the graphitized carbon [68].

The ORR catalytic activity of the thus-synthesized metal-free carbon catalysts was highly comparable to that of Pt/C in both alkaline (Fig. 9c) and acidic electrolytes. Interestingly, such a porous carbon could also efficiently catalyze oxygen evolution reaction (OER), with a potential difference of only 0.806 V between the half-wave potential of ORR and the potential required for achieving an OER current density of 10 mA cm^{-2} in 0.1 M KOH (Fig. 9d). When the best sample 1100-CNS among the series was used as air-

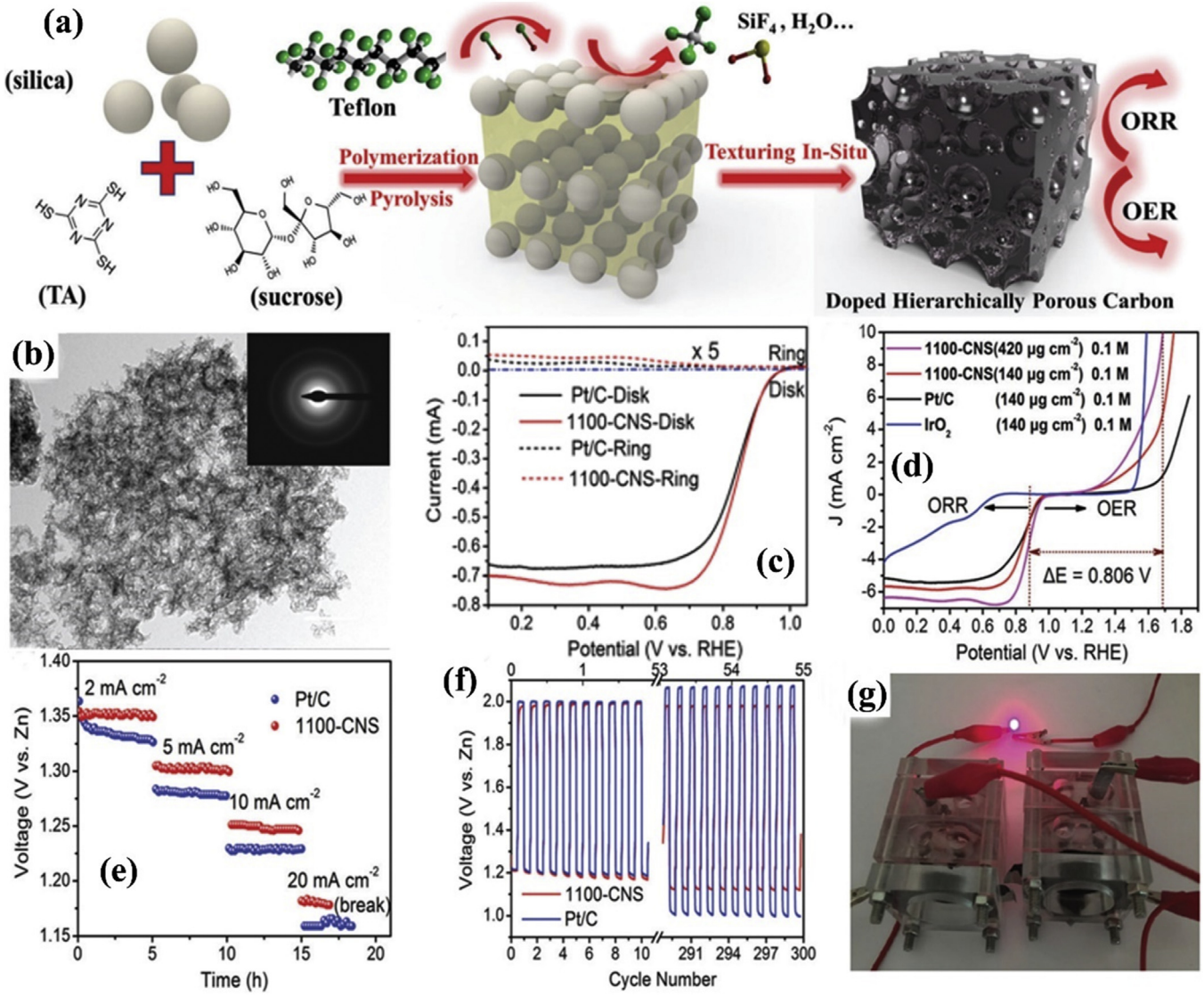

Fig. 9. (a) Illustration of the one-pot fabrication process of doped porous carbon materials. The sucrose and TA precursors were polymerized in the presence of silica followed by Teflon addition. The mixture was pyrolyzed to allow an in situ texturing process, which resulted in N,S as well as O enriched, hierarchically microporous, mesoporous, and macroporous carbon catalysts. (b) TEM observation of the 1100-CNS sample, inset is the selected area electron diffraction (SAED) patterns, scale bar: 200 nm. (c) Electrochemical test for ORR of different samples. (d) LSV curves showing the bifunctional ORR/OER activities of different samples in 0.1 M KOH. (e) Galvanostatic discharge curves of the primary Zn–air battery at different current densities, which were normalized to the area of the air cathode. (f) Rechargeability cycling tests of the Zn–air batteries using the 1100-CNS or Pt/C sample as the catalyst at 10 mA cm^{-2}; (g) photograph showing the lighting of a LED by two Zn–air batteries using 1100-CNS as catalyst in series. Reproduced with permission from the study by Pei et al. [65]. © 2017, Royal Society of Chemistry.

cathode catalysts to assembly a rechargeable Zn-air battery (Fig. 9g), it exhibited a small charge-discharge voltage gap of 0.77 V at 10 mA cm^{-2}, and excellent stability, with an increase of the charge-discharge voltage gap by only 85 mV after 300 cycles at 10 mA cm^{-2}, which surpassed the performance of a reference battery using commercial Pt/C as the cathode catalyst (Fig. 9e–f). The high performance of these porous carbon catalysts clearly demonstrates that this one-pot synthetic strategy is effective in the preparation of efficient oxygen electrocatalysts [69].

2.4. Tellurium-based thermally removable templates

Tellurium is another material that has a relatively low boiling point of 449 °C and hence can serve as a thermally removable template for the synthesis of low-dimensional porous carbons for ORR electrocatalysis [70,71]. For instance, in a recent study [72], we prepared Fe,N-codoped porous carbon nanotubules by controlled pyrolysis of tellurium nanowire (Te NW)–supported melamine formaldehyde polymer core-sheath nanofibers at elevated temperatures. Experimentally, Te NWs were prepared in a hydrothermal procedure with Na_2TeO_3, PVP, and N_2H_4 as the starting materials [73]. A melamine-formaldehyde resin was then grown onto the Te NWs forming a core-sheath structure (Fig. 10a). Controlled pyrolysis at elevated temperatures, with the addition of a calculated amount of $FeCl_3$, led to the formation of Fe,N-codoped carbon nanotubules, while most of Te was evaporated to form a hollow structure. In TEM studies, the resulting hollow carbon nanotubules showed an outer diameter of 35–40 nm, inner diameter of 5–10 nm, and length up to a few hundred nanometers, maintaining a morphology similar to that of the polymer precursors (Fig. 10b–f). The doping of N and Fe into the carbon nanotubules was confirmed by elemental mapping and spectroscopic measurements [74,75]. Specifically, in X-ray photoelectron spectroscopy (XPS) studies, the nitrogen dopants were found to

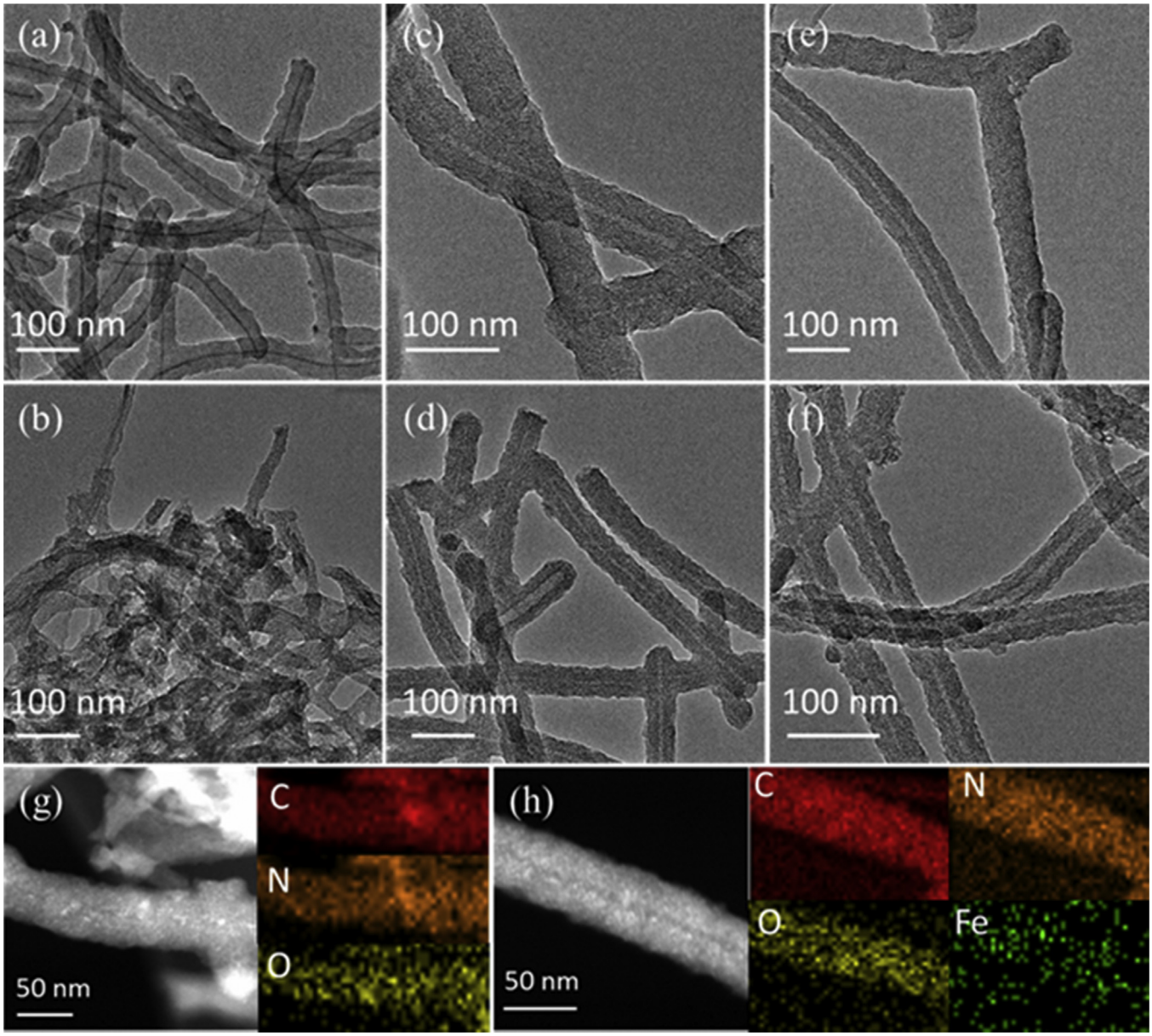

Fig. 10. Representative TEM images of (a) Te-MF, (b) MF-900, (c) MF-Fe-600, (d) MF-Fe-700, (e) MF-Fe-800, and (f) MF-Fe-900. High angle annular dark field scanning transmission electron microscopy (HAADF-STEM) and elemental mapping images of (g) MF-900 and (h) MF-Fe-800. Reprinted with permission from ref. [72]. © 2017, American Chemical Society.

entail various configurations in the carbon matrix, such as pyridinic nitrogen, pyrrolic nitrogen, graphitic nitrogen, oxidized nitrogen, and N in Fe-N, where the Fe-N coordination number was found to be almost invariant at ca. 4.0 for the samples prepared at 600–800 °C but decreased to 1.67 at 900 °C. The resulting Fe,N-codoped carbons exhibited remarkable electrocatalytic activity toward ORR in alkaline media, a performance much enhanced as compared to the control samples doped with nitrogen alone. Among the series, the one prepared at 800 °C exhibited the best performance, with an activity even better than that of Pt/C. We attributed this remarkable performance to the formation of FeN_4 moieties in the carbon matrix that facilitated the binding of oxygen species, a conclusion further supported by results from DFT calculations. Computationally, the ORR performance was systematically studied and compared within the context of graphitic nitrogen-doped carbon and FeN_4-embedded carbon matrix. The results suggested that for carbons doped with N alone, the active sites were the carbon atoms adjacent to nitrogen dopants because of partial electron distribution of the carbon atoms induced by the more electronegative nitrogen dopants, while for Fe,N-codoped carbon, the Fe atoms served as the suitable active sites for the adsorption of oxygen intermediates because of the high spin density of Fe 3d orbital. Significantly, the formation of FeN_4 moieties led to a markedly higher density of states close to the Fermi level and higher spin density, both of which played a critical role in enhancing the electrocatalytic activity.

In a similar manner, Ahn et al. [76] used tellurium nanotubes (Te NTs) as thermally removable templates to prepare Fe,N-containing hierarchical porous carbon framework anchored on porous carbon nanotubes for ORR electrocatalysis. As shown in Fig. 11a, porous Te NTs (Fig. 11b) were used as sacrificial templates as well as substrates for the nucleation and growth of ZIF-8 nanocrystals because Te usually showed strong interactions with a variety of carbonaceous materials, such as dopamine, glucose, and ZIF-8. Experimentally,

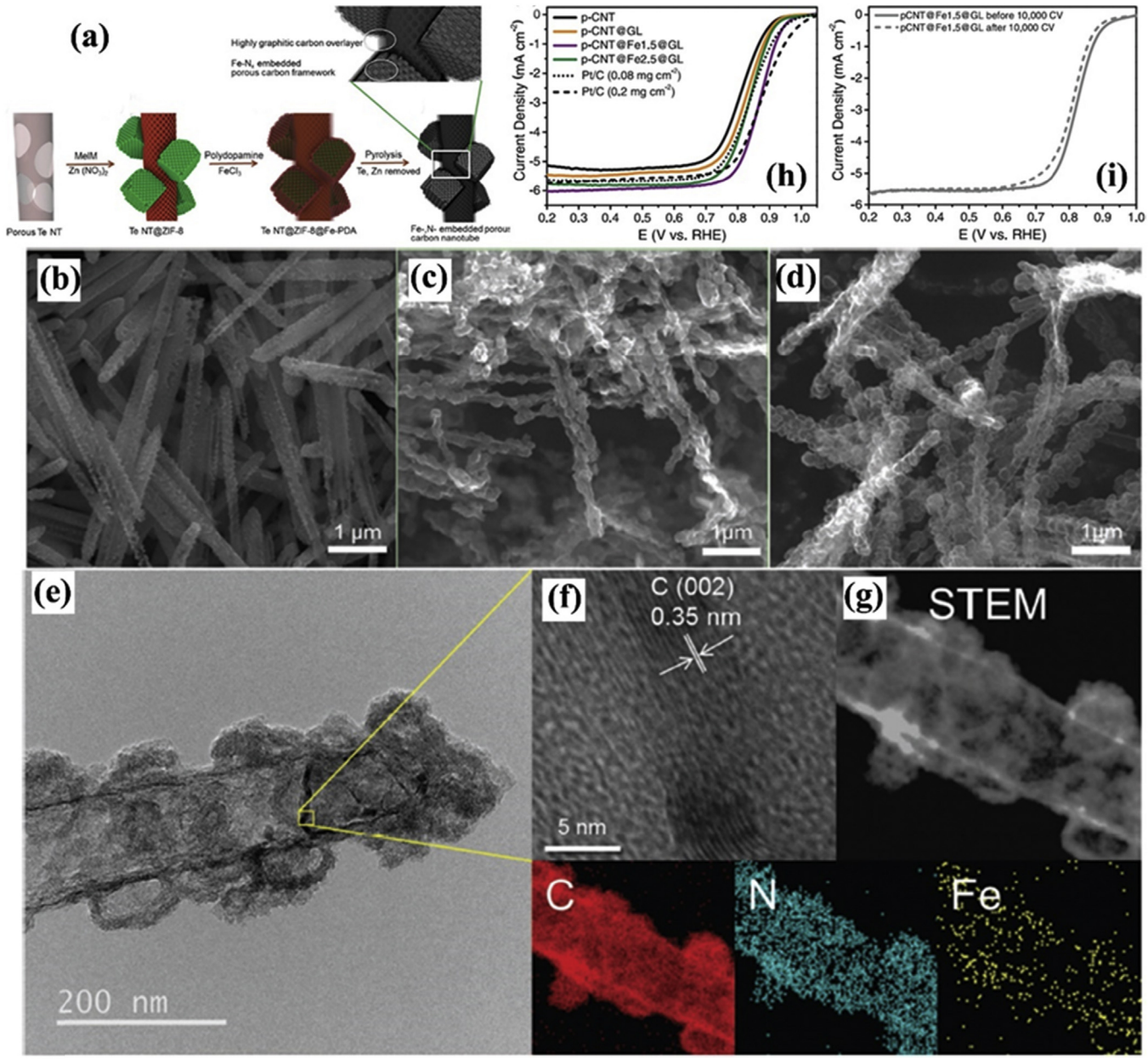

Fig. 11. (a) Schematic illustration of the synthetic method for Fe,N embedded interconnected metal organic framework (MOF)-derived porous carbon nanotubes based on tellurium nanotubes as a sacrificial template. (b) Porous tellurium nanotubes, (c) ZIF-8 wired tellurium nanotubes (Te NT@ZIF-8), (d) Fe,N embedded, polydopamine-coated Te NT@ZIF-8, and (e) Fe,N-embedded, highly graphitic layer coated porous carbon nanotubes after the pyrolysis process at 950 °C for 3 h under argon flow. (f) SEM, TEM, and mapping image for pCNT@Fe1.5%GL. (h) LSV for different samples and Pt/C in O_2-saturated 0.1 M KOH solution at a scan rate of 10 mV s^{-1} at 1600 rpm. (i) LSV curves before (solid line) and after (dashed line) 10 000 cycles from 0.6 VRHE to 1.0 VRHE in O_2-saturated 0.1 m $HClO_4$ at 50 mV s^{-1}. Reprinted with permission from the study by Ahn et al. [76]. ©2017, Wiley-VCH Verlag GmbH & Co. KGaA.

these porous Te NTs templates were prepared from tellurium oxide nanoparticles by an in situ reduction and etching method in the presence of sodium hydroxide and ammonia, which were used as reductant and etching reagents, respectively. Subsequently, the Zn-containing ZIF-8 MOF nanocrystals were in situ grown on the surface of porous Te NTs (Fig. 11c), followed by in situ polymerization of dopamine at room temperature in the aqueous solution of $FeCl_3$. This thin polydopamine (PDA) layer was coordinated to Fe^{3+}, which was converted to FeN_xC active sites embedded in the eventual carbon framework after pyrolysis [77], thereby generating an ultrathin PDA-derived Fe, N-codoped graphitized carbon overlayer. Similar to the aforementioned Zn-containing templates, elemental Zn in ZIF-8 nanocrystals was reduced to Zn^0 by carbon during high-temperature pyrolysis in the inert atmosphere. The in situ formed Zn^0 and Te NTs were gradually evaporated, which promoted the formation of porous structures on a shish kebab–like carbon composite material where discrete nanoparticles with hierarchical pores were wired on the surface of mesoporous carbon nanotubes (Fig. 11d–g).

This morphology is highly beneficial to the ORR electrocatalysis. The support from mesoporous carbon nanotube helped prevent the aggregation of MOF-derived porous carbon nanoparticles and homogeneously distribute Fe and N elements on the porous carbon matrix to form active sites [78]. Therefore, the mass transport process in these unique carbon catalysts was promoted, and the exposure of active sites was maximized. Also, the presence of a

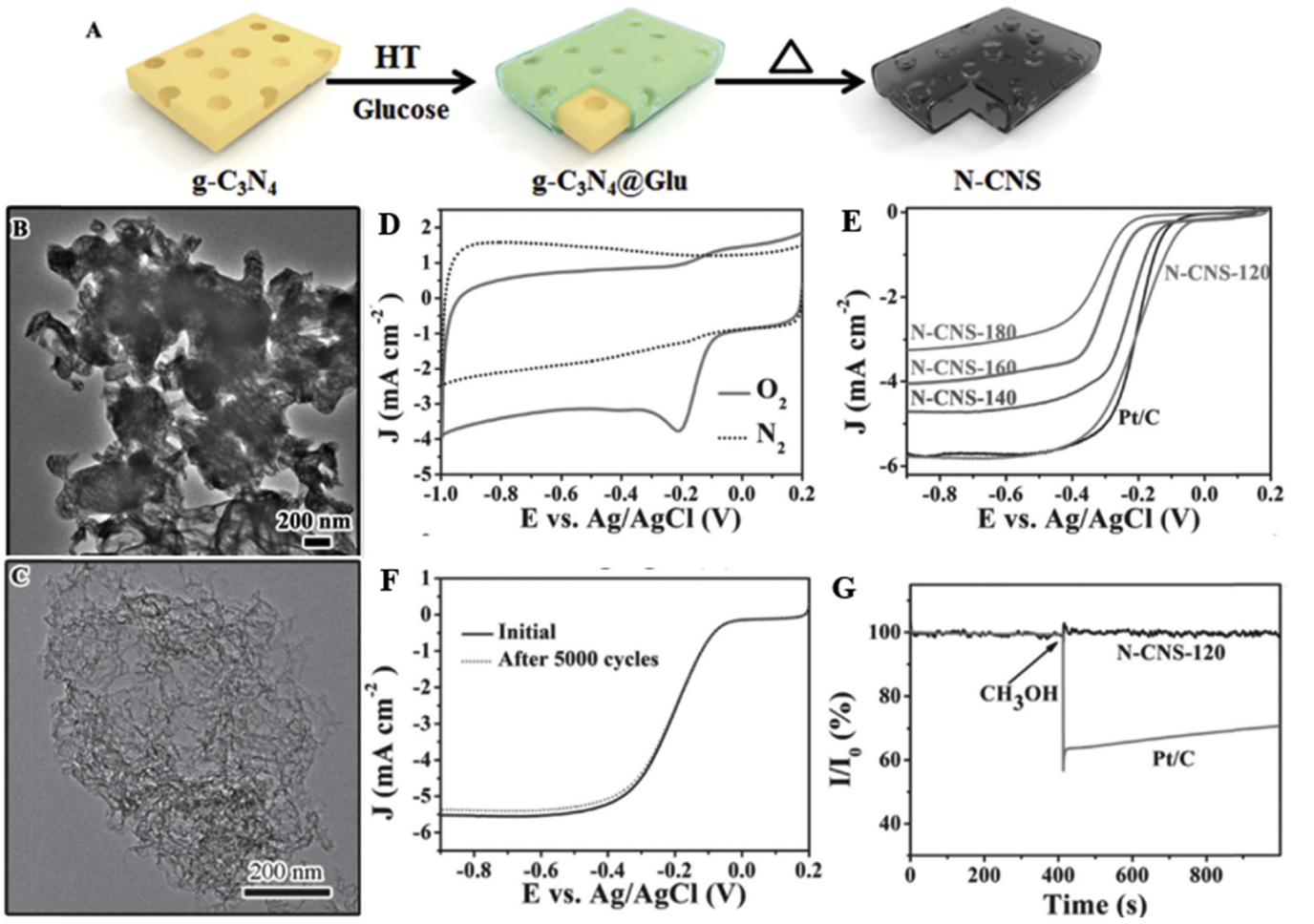

Fig. 12. (a) Schematic for the synthesis of N-CNS templated from g-C_3N_4; TEM images of (b) g-C_3N_4, (c) N-CNS-120, (d) Cyclic voltammetry (CV) curves of N-CNS-120 in N_2 and O_2 saturated 0.1 M KOH aqueous solution with a scan rate of 50 mV s−1. (e) LSV curves of all N-CNS-t and Pt/C in O_2-saturated 0.1 M KOH electrolyte with a scan rate of 10 mV s−1 and a rotation rate of 1600 rpm. (f) LSV curves of N-CNS-120 before and after cycling for 5000 cycles with a rotation rate of 1600 rpm. (g) The durability test of N-CNS-120 and Pt/C for methanol. Reprinted with permission from the study by Yu et al. [83]. © 2016, Wiley-VCH Verlag GmbH & Co. KGaA.

highly graphitized carbon overlayer protected the catalytic active sites from aggregation and corrosion in operation conditions, which increased the long-term stability of the catalyst. In addition, the highly conductive carbon nanotubes provided effective pathways for electron transfer. Indeed, the resulting catalyst demonstrated a high specific surface area of 1380 $cm^2\ g^{-1}$ and a high ORR electrocatalytic activity in both alkaline and acidic electrolytes, as compared with commercial Pt/C. The long-term stability was also remarkable, highlighting the advantages of PDA-derived graphitized carbon overlayer in facilitating the ORR electron-transfer and mass-transfer dynamics.

In another study [46], Manthiram et al. used the similar synthesis route to prepare 1D, hierarchically porous carbon nanotubes dually doped with N and Co, which were also found to exhibit efficient electrocatalytic activity toward ORR.

2.5. Carbon nitride–based templates

Graphitic carbon nitride (g-C_3N_4) refers to a family of carbon nitride compounds with a stoichiometric ratio of C:N ≈ 3:4. There are two main substructures based on heptazine and poly(triazine imide) repeating units with a different degree of condensation. g-C_3N_4 can be synthesized thermally by polymerization of cyanamide, dicyandiamide, or melamine at about 530 °C in an inert atmosphere [79–81]. However, a further increase of the heating temperature causes the decomposition of g-C_3N_4, and at temperatures higher than 680 °C, g-C_3N_4 can be completely decomposed into volatile compounds without any residuals probably by the reaction of $2C_3N_4(s) \rightarrow 3NC\text{-}CN(g) + N_2(g)$, as evidenced in thermogravimetric analysis (TGA) measurements [82]. Therefore, g-C_3N_4 can also serve as thermally removable templates for the preparation of low-dimensional porous carbon catalysts.

For instance, Zhang's group reported the preparation of nitrogen-doped, (micro- and meso-)porous carbon nanosheets (N-CNS) as a highly efficient ORR electrocatalyst, which exhibited a high specific surface area and a high content of nitrogen, by using glucose as the carbon precursor and g-C_3N_4 as both the thermally removable template and nitrogen source in a hydrothermal plus carbonization procedure (Fig. 12a–c) [83]. The resulting N-CNS catalyst showed a high nitrogen content of 11.6 at.% and a specific surface area of 1077 $m^2\ g^{-1}$, apparent ORR catalytic performance (Fig. 12d–e), and high working stability and strong tolerance to fuel crossover (Fig. 12f–g). In another study, Li et al. [84] prepared N-doped porous carbon sheets for ORR electrocatalysis via direct carbonization of protonated g-C_3N_4 (p-g-C_3N_4) and PPy. In this synthesis route, the p-g-C_3N_4 was used to firmly attract pyrrole monomers because of its lone electron pairs so that polymerization of pyrrole could homogeneously occur, and the resulting polypyrrole was deposited on the p-g-C_3N_4 surface. Similarly, during the subsequent pyrolysis process, p-g-C_3N_4 acted as a sacrificial

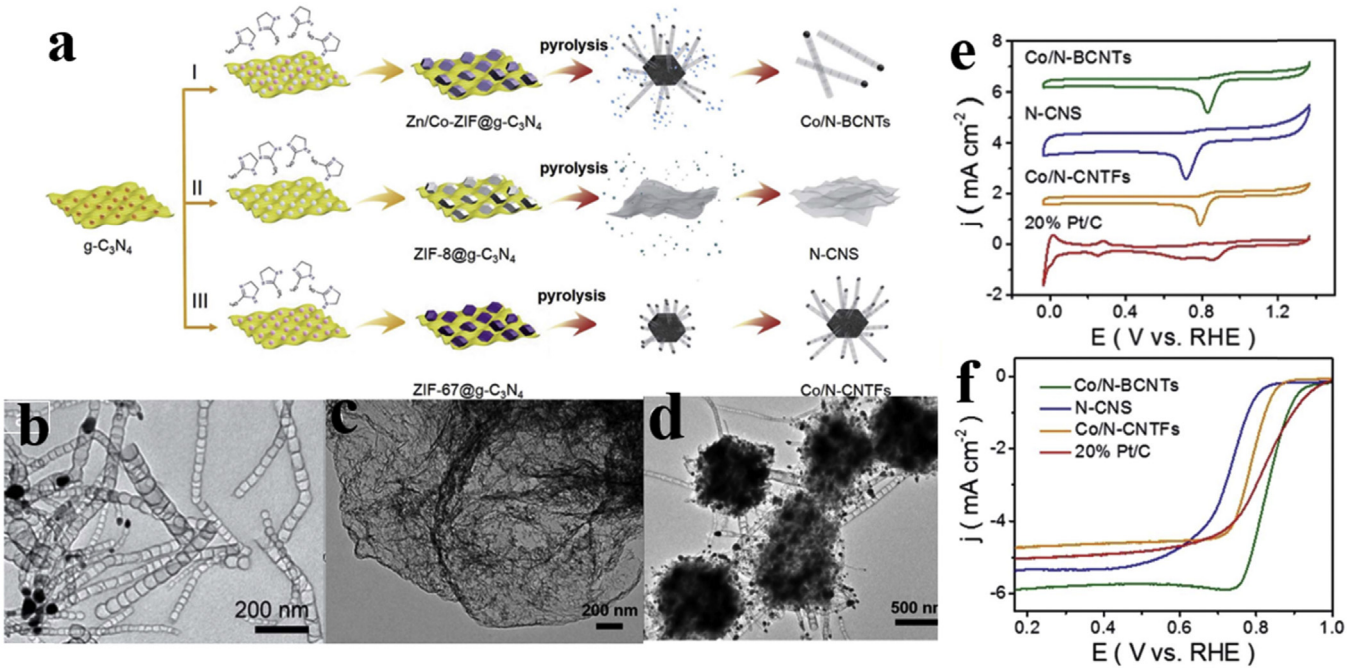

Fig. 13. (a) Schematic illustration of the preparation of nitrogen-doped carbon nanomaterials; TEM image of (b) Co/N-BCNTs, (c) N-CNS, and (d) Co/N-CNTFs; (e) CV curves of all catalysts in O_2-saturated 0.1 M KOH solution; (f) LSV curves in an O2-saturated 0.1 M KOH solution at a sweep rate of 10 mV s^{-1} and electrode rotation speed of 1600 rpm. Reproduced with permission from the study by Wang et al. [86]. BCNTs, bamboo-like CNTs. ©2018, Royal Society of Chemistry.

template and also nitrogen sources, resulting in a high N content (mainly pyridinic and graphitic N) and large specific surface area (1716 m^2 g^{-1}). g-C_3N_4 was also used by Lv et al. [85] to prepare oxygen species–modified N-doped carbon nanosheets (O–N–CNs), which displayed epoxy oxygen and ketene oxygen as well as graphitic-nitrogen defects. With abundant active sites for ORR, electrochemical studies showed an excellent ORR activity with a half-wave potential of +0.87 V vs RHE.

In a more recent study, Wang et al. [86] in situ grew ZIF arrays on g-C_3N_4 nanosheets to synthesize Co nanoparticle-encapsulated 1D N-doped bamboo-like CNTs (Co/N-BCNTs) and 3D N-doped CNT framework (Co/N-CNTFs), as well as Co nanoparticle-free 2D N-doped carbon nanosheets (N-CNS) (Fig. 13a–d) by a pyrolysis process. In this strategy, g-C_3N_4 not only served as a nitrogen source but also as a template attracting positive metal ions because of its negative charge on the surface, and therefore, ZIFs nanoparticles could be in situ grown onto the g-C_3N_4 nanosheets. The best Co/NBCNTs electrocatalyst even outperformed commercial Pt/C catalyst (20 wt%) towards ORR (Fig. 13e–f), with a half-wave potential of +0.83 V vs. RHE in alkaline electrolytes.

Jia's group also observed excellent ORR activity with graphene-like N-doped carbon nanosheets (thickness 0.6–2 nm) prepared via a one-step, solvent-free method. In this method, dicyandiamide was used to fabricate layered g-C_3N_4, which then served as a sacrificial template and confined the condensation polymerization of dopamine, affording 2D N-doped carbon nanosheets [87]. This dopamine-derived graphene-like carbon nanosheets exhibited a large specific surface area and an excellent ORR activity in both alkaline and acidic media (E_{onset} = +0.94 V, and $E_{1/2}$ = +0.85 V).

3. Conclusions and outlook

In summary, a variety of nanostructures have been exploited as thermally removable templates to in situ control the porosity of low-dimensional heteroatom-doped carbons that have shown apparent electrocatalytic activity towards ORR. This is primarily due to the relatively low boiling points that render it possible for the materials to become volatile at pyrolysis temperatures, such that the evaporation results in the formation of a hierarchically porous structure. This is significant for the ORR performance of the carbon catalysts, as porosity dictates the specific surface area and hence the accessibility of the catalytic active sites. Meanwhile, the pore size and volume control the transport of oxygen and reaction intermediates, where mesopores have been recognized to be the optimal size range that facilitates the mass transfer dynamics of ORR. Thus, one can envisage that structural engineering of the porous carbon catalysts plays a critical role in the manipulation, and ultimately optimization, of the ORR performance.

Despite substantial progress, much remains to be accomplished. First, as highlighted in the previous section, the choices of thermally removable templates have been rather limited. Further research is desired to identify appropriate materials that exhibit a relatively low boiling point and can form a somewhat robust structure that may serve as a supporting scaffold to sustain the carbon skeletons during pyrolysis. In particular, indirect removable templates such as the SiO_2-HF approach described previously are anticipated to offer a unique control of the loading of template porogens by, for instance, stoichiometric feeding, and hence the final porosity of the carbon catalysts.

While the dimensions of the pores appear to be somewhat correlated with the size of the thermally removable templates, no systematic studies have been carried out to unravel the mechanistic insights. This is largely due to the complicated reaction processes involved in high-temperature carbonization (e.g., Eqs (1–12)). Ideally, if the correlation between the pore size and (thermally removable or otherwise) template dimensions is clearly defined, one can then tailor the carbon structures by a predesigned template. This remains a challenge.

Furthermore, one may notice that the thermally removable templates, as exemplified in the section above, can be used to prepare single metal atom catalysts. This is to take advantage of the volatility of the metal species such that only a trace amount

remains and become atomically dispersed in the carbon matrix during pyrolysis. However, so far, only non-noble metal compounds have been used and the electrocatalytic activity, while remarkable, remains mostly subpar as compared to that of Pt/C. Therefore, one may ask, is it possible to extend the chemistry to noble metals, such as Pt, Pd, Ru, Rh, and so forth, which exhibit remarkable electrocatalytic activity even at the single atom levels for a diverse range of reactions [88]. This will be an interesting area of research.

Declarations of interest

The authors have no conflict of interest to disclose.

Data Availability

Data presented in this paper are reproduced with permission from the respective publishers. They can be requested from the original authors.

Acknowledgments

This work was supported by the National Natural Science Foundation of China (Nos. 21528301 and 51402111), Guangdong Innovative and Entrepreneurial Research Team Program (No. 2014ZT05N200), and the Fundamental Research Funds for Central Universities (No. 2018ZD21). S.W.C. thanks the US National Science Foundation for partial support of the work (CHE-1710408 and CBET-1848841).

References

[1] D. Guo, R. Shibuya, C. Akiba, S. Saji, T. Kondo, J. Nakamura, Active sites of nitrogen-doped carbon materials for oxygen reduction reaction clarified using model catalysts, Science 351 (6271) (2016) 361–365.
[2] L. Dai, Y. Xue, L. Qu, H.-J. Choi, J.-B. Baek, Metal-free catalysts for oxygen reduction reaction, Chem. Rev. 115 (11) (2015) 4823–4892.
[3] F. Cheng, J. Chen, Metal–air batteries: from oxygen reduction electrochemistry to cathode catalysts, Chem. Soc. Rev. 41 (6) (2012) 2172–2192.
[4] D. Banham, S. Ye, K. Pei, J.-i. Ozaki, T. Kishimoto, Y. Imashiro, A review of the stability and durability of non-precious metal catalysts for the oxygen reduction reaction in proton exchange membrane fuel cells, J. Power Sources 285 (2015) 334–348.
[5] X.X. Wang, D.A. Cullen, Y.T. Pan, S. Hwang, M. Wang, Z. Feng, J. Wang, M.H. Engelhard, H. Zhang, Y. He, Nitrogen-coordinated single cobalt atom catalysts for oxygen reduction in proton exchange membrane fuel cells, Adv. Mater 30 (11) (2018), 1706758.
[6] D. Zhao, J. Dai, N. Zhou, N. Wang, X. Peng, Y. Qu, l. Li, Prussian blue analogues-derived carbon composite with cobalt nanoparticles as an efficient bifunctional electrocatalyst for oxygen reduction and hydrogen evolution, Carbon 142 (2019) 196–205.
[7] S. Shen, T. Zhao, J. Xu, Y. Li, Synthesis of PdNi catalysts for the oxidation of ethanol in alkaline direct ethanol fuel cells, J. Power Sources 195 (4) (2010) 1001–1006.
[8] S. Ratso, I. Kruusenberg, A. Sarapuu, P. Rauwel, R. Saar, U. Joost, J. Aruväli, P. Kanninen, T. Kallio, K. Tammeveski, Enhanced oxygen reduction reaction activity of iron-containing nitrogen-doped carbon nanotubes for alkaline direct methanol fuel cell application, J. Power Sources 332 (2016) 129–138.
[9] S.S. Shinde, H.L. Chi, J.Y. Yu, D.H. Kim, U.L. Sang, J.H. Lee, Hierarchically designed 3D holey C2N aerogels as bifunctional oxygen electrodes for flexible and rechargeable Zn-air batteries, ACS Nano 12 (1) (2017) 596–608.
[10] P. Cai, S. Ci, E. Zhang, P. Shao, C. Cao, Z. Wen, FeCo alloy nanoparticles confined in carbon layers as high-activity and robust cathode catalyst for Zn-air battery, Electrochim. Acta 220 (2016) 354–362.
[11] K. Marcus, K. Liang, W. Niu, Y. Yang, Nickel sulfide freestanding holey films as air-breathing electrodes for flexible Zn-air batteries, J. Phys. Chem. Lett. 9 (11) (2018) 2746–2750.
[12] H.B. Yang, J. Miao, S.F. Hung, J. Chen, H.B. Tao, X. Wang, L. Zhang, R. Chen, J. Gao, H.M. Chen, Identification of catalytic sites for oxygen reduction and oxygen evolution in N-doped graphene materials: development of highly efficient metal-free bifunctional electrocatalyst, Sci. Adv. 2 (4) (2016) e1501122-e1501122.
[13] A.M. El-Sawy, I.M. Mosa, D. Su, C.J. Guild, S. Khalid, R. Joesten, J.F. Rusling, S.L. Suib, Controlling the active sites of sulfur-doped carbon nanotube–graphene nanolobes for highly efficient oxygen evolution and reduction catalysis, Adv. Energy Mater. 6 (5) (2016), 1501966.
[14] C. Huang, T. Ouyang, Y. Zou, N. Li, Z.-Q. Liu, Ultrathin NiCo 2 P x nanosheets strongly coupled with CNTs as efficient and robust electrocatalysts for overall water splitting, J. Mater. Chem. A 6 (17) (2018) 7420–7427.
[15] J. Wang, Z. Wu, L. Han, R. Lin, W. Xiao, C. Xuan, H.L. Xin, D. Wang, Nitrogen and sulfur co-doping of partially exfoliated MWCNTs as 3-D structured electrocatalysts for the oxygen reduction reaction, J. Mater. Chem. A 4 (15) (2016) 5678–5684.
[16] Y. Hou, T. Huang, Z. Wen, S. Mao, S. Cui, J. Chen, Metal–Organic framework-derived nitrogen-doped core-shell-structured porous Fe/Fe 3 C@C nanoboxes supported on graphene sheets for efficient oxygen reduction reactions, Adv. Energy Mater. 4 (11) (2014) 1220–1225.
[17] W. Niu, L. Li, S. Chen, Recent progress in template-assisted synthesis of nitrogen-doped porous carbons for oxygen electroreduction, J. Electrochem. 23 (2) (2017) 110–122.
[18] J.L. Dong, U.N. Maiti, J. Lim, S.C. Dong, W.J. Lee, Y. Oh, G.Y. Lee, O.K. Sang, Molybdenum sulfide/N-doped CNT forest hybrid catalysts for high-performance hydrogen evolution reaction, Nano. Lett. 14 (3) (2014) 1228–1233.
[19] D. Zhao, L. Li, L. Xie, N. Zhou, S. Chen, Sulfur codoping enables efficient oxygen electroreduction on FeCo alloy encapsulated in N-Doped carbon nanotubes, J. Alloy. Comp. 741 (2018) 368–376.
[20] J. Zhang, H. Zhou, X. Liu, J. Zhang, T. Peng, J. Yang, Y. Huang, S. Mu, Keratin-derived S/N co-doped graphene-like nanobubble and nanosheet hybrids for highly efficient oxygen reduction, J. Mater. Chem. A 4 (41) (2016) 15870–15879.
[21] N. Wang, L. Li, D. Zhao, X. Kang, Z. Tang, S. Chen, Graphene composites with cobalt sulfide: efficient trifunctional electrocatalysts for oxygen reversible catalysis and hydrogen production in the same electrolyte, Small 13 (33) (2017) 1701025.
[22] C. Zhang, B. An, L. Yang, B. Wu, W. Shi, Y.-C. Wang, L.-S. Long, C. Wang, W. Lin, Sulfur-doping achieves efficient oxygen reduction in pyrolyzed zeolitic imidazolate frameworks, J. Mater. Chem. A 4 (12) (2016) 4457–4463.
[23] M. Borghei, N. Laocharoen, E. Kibena-Põldsepp, L.-S. Johansson, J. Campbell, E. Kauppinen, K. Tammeveski, O.J. Rojas, N. Porous, P-doped carbon from coconut shells with high electrocatalytic activity for oxygen reduction: alternative to Pt-C for alkaline fuel cells, Appl. Catal. B Environ. 204 (2017) 394–402.
[24] J. Wang, J. Hao, D. Liu, S. Qin, D. Portehault, Y. Li, Y. Chen, W. Lei, Porous boron carbon nitride nanosheets as efficient metal-free catalysts for the oxygen reduction reaction in both alkaline and acidic solutions, ACS Energy Lett. 2 (2) (2017) 306–312.
[25] Y. Hou, S. Cui, Z. Wen, X. Guo, X. Feng, J. Chen, Strongly coupled 3D hybrids of N-doped porous carbon nanosheet/CoNi alloy-encapsulated carbon nanotubes for enhanced electrocatalysis, Small 11 (44) (2015) 5940–5948.
[26] M. Shen, C. Wei, K. Ai, L. Lu, Transition metal–nitrogen–carbon nanostructured catalysts for the oxygen reduction reaction: from mechanistic insights to structural optimization, Nano. Res. 10 (5) (2017) 1449–1470.
[27] X. Liu, M. Park, M.G. Kim, S. Gupta, G. Wu, J. Cho, Integrating NiCo alloys with their oxides as efficient bifunctional cathode catalysts for rechargeable zinc-air batteries, Angew. Chem. Int. Ed. 54 (33) (2015) 9654–9658.
[28] C. Hu, L. Dai, Carbon-based metal-free catalysts for electrocatalysis beyond the ORR, Angew. Chem. Int. Ed. 55 (39) (2016) 11736–11758.
[29] T. Meng, J. Qin, S. Wang, D. Zhao, B. Mao, M. Cao, In situ coupling of Co 0.85 Se and N-doped carbon via one-step selenization of metal–organic frameworks as a trifunctional catalyst for overall water splitting and Zn–air batteries, J. Mater. Chem. A 5 (15) (2017) 7001–7014.
[30] N. Wang, B. Lu, L. Li, W. Niu, Z. Tang, X. Kang, S. Chen, Graphitic N is responsible for oxygen electroreduction on N-doped carbons in alkaline electrolytes: insights from activity attenuation studies and theoretical calculations, ACS Catal. 8 (8) (2018) 6827–6836.
[31] R. Silva, D. Voiry, M. Chhowalla, T. Asefa, Efficient metal-free electrocatalysts for oxygen reduction: polyaniline-derived N-and O-doped mesoporous carbons, J. Am. Chem. Soc. 135 (21) (2013) 7823–7826.
[32] X. Liu, Y. Zhou, W. Zhou, L. Li, S. Huang, S. Chen, Biomass-derived nitrogen self-doped porous carbon as effective metal-free catalysts for oxygen reduction reaction, Nanoscale 7 (14) (2015) 6136–6142.
[33] S. Li, C. Cheng, X. Zhao, J. Schmidt, A. Thomas, Active salt/silica-templated 2D mesoporous FeCo-Nx-Carbon as bifunctional oxygen electrodes for zinc–air batteries, Angew. Chem. Int. Ed. 57 (7) (2018) 1856–1862.
[34] M. Zhang, Q. Dai, H. Zheng, M. Chen, L. Dai, Novel MOF-derived Co@ N-C bifunctional catalysts for highly efficient Zn–air batteries and water splitting, Adv Mater 30 (10) (2018), 1705431.
[35] S. Dou, X. Li, L. Tao, J. Huo, S. Wang, Cobalt nanoparticle-embedded carbon nanotube/porous carbon hybrid derived from MOF-encapsulated Co 3 O 4 for oxygen electrocatalysis, Chem. Commun. 52 (62) (2016) 9727–9730.
[36] Q. Ren, H. Wang, X.F. Lu, Y.X. Tong, G.R. Li, Recent progress on MOF-derived heteroatom-doped carbon-based electrocatalysts for oxygen reduction reaction, Adv. Sci. 5 (3) (2018), 1700515.
[37] H.-W. Liang, S. Brüller, R. Dong, J. Zhang, X. Feng, K. Müllen, Molecular metal–N x centres in porous carbon for electrocatalytic hydrogen evolution, Nat. Commun. 6 (2015) 7992.

[38] C. Liang, Z. Li, S. Dai, Mesoporous carbon materials: synthesis and modification, Angew. Chem. Int. Ed. 47 (20) (2008) 3696–3717.
[39] F. Wang, S. Song, K. Li, J. Li, J. Pan, S. Yao, X. Ge, J. Feng, X. Wang, H. Zhang, A "solid dual-ions-transformation" route to S,N Co-doped carbon nanotubes as highly efficient "Metal-Free" catalysts for organic reactions, Adv. Mater. 28 (48) (2016) 10679–10683.
[40] H. Zhao, C.C. Weng, Z.P. Hu, L. Ge, Z.Y. Yuan, CdS-polydopamine derived N, S co-doped hierarchically porous carbons as highly active electrocatalyst for oxygen reduction, ACS Sustain. Chem. Eng. 5 (11) (2017) 9914–9922.
[41] W. Niu, L. Li, X. Liu, N. Wang, J. Liu, W. Zhou, Z. Tang, S. Chen, Mesoporous N-doped carbons prepared with thermally removable nanoparticle templates: an efficient electrocatalyst for oxygen reduction reaction, J. Am. Chem. Soc. 137 (16) (2015) 5555–5562.
[42] J. Liu, L.G. Li, W.H. Niu, N. Wang, D.K. Zhao, S.B. Zeng, S.W. Chen, A hydrogen-bonded organic-framework-derived mesoporous N-doped carbon for efficient electroreduction of oxygen, Chemelectrochem 3 (7) (2016) 1116–1123.
[43] P.C. Shi, J.D. Yi, T.T. Liu, L. Li, L.J. Zhang, C.F. Sun, Y.B. Wang, Y.B. Huang, R. Cao, Hierarchically porous nitrogen-doped carbon nanotubes derived from core-shell ZnO@zeolitic imidazolate framework nanorods for highly efficient oxygen reduction reactions, J. Mater. Chem. A 5 (24) (2017) 12322–12329.
[44] Y.Z. Chen, C. Wang, Z.Y. Wu, Y. Xiong, Q. Xu, S.H. Yu, H.L. Jiang, Metal-organic frameworks: from bimetallic metal-organic framework to porous carbon: high surface area and multicomponent active dopants for excellent electrocatalysis, Adv. Mater. 27 (34) (2015) 5010–5016.
[45] Z.H. Li, M.F. Shao, L. Zhou, Q.H. Yang, C. Zhang, M. Wei, D.G. Evans, X. Duan, Carbon-based electrocatalyst derived from bimetallic metal-organic framework arrays for high performance oxygen reduction, Nano. Energy 25 (2016) 100–109.
[46] S.H. Ahn, M.J. Klein, A. Manthiram, 1D Co- and N-doped hierarchically porous carbon nanotubes derived from bimetallic metal organic framework for efficient oxygen and tri-iodide reduction reactions, Adv. Energy Mater. 7 (7) (2017), 1601979.
[47] C. Lin, S.S. Shinde, Z. Jiang, X.K. Song, Y. Sun, L.L. Guo, H. Zhang, J.Y. Jung, X.P. Li, J.H. Lee, In situ directional formation of Co@CoOx-embedded 1D carbon nanotubes as an efficient oxygen electrocatalyst for ultra-high rate Zn-air batteries, J. Mater. Chem. A 5 (27) (2017) 13994–14002.
[48] S.G. Wang, Z.T. Cui, J.W. Qin, M.H. Cao, Thermally removable in-situ formed ZnO template for synthesis of hierarchically porous N-doped carbon nanofibers for enhanced electrocatalysis, Nano. Res. 9 (8) (2016) 2270–2283.
[49] Y. Xiao, P. Sun, M. Cao, Core–shell bimetallic carbide nanoparticles confined in a three-dimensional N-doped carbon conductive network for efficient lithium storage, ACS Nano. 8 (8) (2014) 7846–7857.
[50] J. Liang, Y. Zheng, J. Chen, J. Liu, D. Hulicovajurcakova, M. Jaroniec, S.Z. Qiao, Facile oxygen reduction on a three-dimensionally ordered macroporous graphitic C3N4/carbon composite electrocatalyst, Angew. Chem. Int. Ed. 51 (16) (2012) 3892–3896.
[51] J. Liang, X. Du, C. Gibson, X.W. Du, S.Z. Qiao, N-Doped graphene natively grown on hierarchical ordered porous carbon for enhanced oxygen reduction, Adv. Mater. 25 (43) (2013) 6226–6231.
[52] X. Zhong, L. Liu, Y. Jiang, X. Wang, L. Wang, G. Zhuang, X. Li, D. Mei, J.g. Wang, D.S. Su, Synergistic effect of nitrogen in cobalt nitride and nitrogen-doped hollow carbon spheres for the oxygen reduction reaction, ChemCatChem 7 (12) (2015) 1826–1832.
[53] C. Li, Z. Li, Z. Cheng, X. Ding, J. Zhang, R. Huang, L. Qu, Functional carbon nanomesh clusters, Adv. Funct. Mater. 27 (30) (2017), 1701514.
[54] S. Yadnum, J. Roche, E. Lebraud, P. Nã©Grier, P. Garrigue, D. Bradshaw, C. Warakulwit, J. Limtrakul, A. Kuhn, Site-selective synthesis of Janus-type metal-organic framework composites, Angew. Chem. Int. Ed. 126 (15) (2014) 4001–4005.
[55] H. Yang, S.J. Bradley, A. Chan, G.I. Waterhouse, T. Nann, P.E. Kruger, S.G. Telfer, Catalytically active bimetallic nanoparticles supported on porous carbon capsules derived from metal–organic framework composites, J. Am. Chem. Soc. 138 (36) (2016) 11872–11881.
[56] E. Zhang, Y. Xie, S. Ci, J. Jia, P. Cai, L. Yi, Z. Wen, Multifunctional high-activity and robust electrocatalyst derived from metal–organic frameworks, J. Mater. Chem. 4 (44) (2016) 17288–17298.
[57] W. Niu, L. Li, J. Liu, N. Wang, W. Li, Z. Tang, W. Zhou, S. Chen, Graphene-supported mesoporous carbons prepared with thermally removable templates as efficient catalysts for oxygen electroreduction, Small 12 (14) (2016) 1900–1908.
[58] S. Yang, X. Feng, X. Wang, K. Müllen, Graphene-based carbon nitride nanosheets as efficient metal-free electrocatalysts for oxygen reduction reactions, Angew. Chem. Int. Ed. 123 (23) (2011) 5451–5455.
[59] X. Zhou, J. Qiao, L. Yang, J. Zhang, A review of graphene-based nanostructural materials for both catalyst supports and metal-free catalysts in PEM fuel cell oxygen reduction reactions, Adv. Energy Mater. 4 (8) (2014), 1301523.
[60] W. He, C. Jiang, J. Wang, L. Lu, High-rate oxygen electroreduction over graphitic-N species exposed on 3D hierarchically porous nitrogen-doped carbons, Angew. Chem. Int. Ed. 53 (36) (2014) 9503–9507.
[61] B. Men, Y. Sun, J. Liu, Y. Tang, Y. Chen, P. Wan, J. Pan, Synergistically enhanced electrocatalytic activity of sandwich-like N-doped graphene/carbon nanosheets decorated by Fe and S for oxygen reduction reaction, ACS Appl. Mater. Interfaces 8 (30) (2016) 19533–19541.
[62] H. Wang, N. Yang, W. Li, W. Ding, K. Chen, J. Li, L. Li, J. Wang, J. Jiang, F. Jia, Understanding the roles of nitrogen configurations for hydrogen evolution: trace atomic cobalt boost the activity of planar nitrogen doped graphene, ACS Energy Lett. 3 (6) (2018) 1345–1352.
[63] B. Chen, Z. Jiang, L. Zhou, B. Deng, Z.-J. Jiang, J. Huang, M. Liu, Electronic coupling induced high performance of N, S-codoped graphene supported CoS 2 nanoparticles for catalytic reduction and evolution of oxygen, J. Power Sources 389 (2018) 178–187.
[64] W. Niu, L. Li, N. Wang, S. Zeng, J. Liu, D. Zhao, S. Chen, Volatilizable template-assisted scalable preparation of honeycomb-like porous carbons for efficient oxygen electroreduction, J. Mater. Chem. A 4 (28) (2016) 10820–10827.
[65] Z. Pei, H. Li, Y. Huang, Q. Xue, Y. Huang, M. Zhu, Z. Wang, C. Zhi, Texturing in situ: N,S-enriched hierarchically porous carbon as a highly active reversible oxygen electrocatalyst, Energy Environ. Sci. 10 (3) (2017) 742–749.
[66] J.A. Conesa, R. Font, Polytetrafluoroethylene decomposition in air and nitrogen, Polym. Eng. Sci. 41 (12) (2001) 2137–2147.
[67] H.W. Liang, X. Zhuang, S. Brüller, X. Feng, K. Müllen, Hierarchically porous carbons with optimized nitrogen doping as highly active electrocatalysts for oxygen reduction, Nat. Commun. 5 (5) (2014) 4973.
[68] I.S. Amiinu, Z. Pu, X. Liu, K.A. Owusu, H.G.R. Monestel, F.O. Boakye, H. Zhang, S. Mu, Multifunctional Mo–N/C@ MoS2 electrocatalysts for HER, OER, ORR, and Zn–air batteries, Adv. Funct. Mater. 27 (44) (2017), 1702300.
[69] T. Liu, F. Yang, G. Cheng, W. Luo, Reduced graphene oxide-wrapped Co9–xFexS8/Co, Fe-N-C composite as bifunctional electrocatalyst for oxygen reduction and evolution, Small 14 (10) (2018), 1703748.
[70] H.-W. Liang, J.-W. Liu, H.-S. Qian, S.-H. Yu, Multiplex templating process in one-dimensional nanoscale: controllable synthesis, macroscopic assemblies, and applications, Acc. Chem. Res. 46 (7) (2013) 1450–1461.
[71] L.-T. Song, Z.-Y. Wu, H.-W. Liang, F. Zhou, Z.-Y. Yu, L. Xu, Z. Pan, S.-H. Yu, Macroscopic-scale synthesis of nitrogen-doped carbon nanofiber aerogels by template-directed hydrothermal carbonization of nitrogen-containing carbohydrates, Nano. Energy 19 (2016) 117–127.
[72] B. Lu, T.J. Smart, D. Qin, J.E. Lu, N. Wang, L. Chen, Y. Peng, Y. Ping, S. Chen, Nitrogen and iron-codoped carbon hollow nanotubules as high-performance catalysts towards oxygen reduction reaction: a combined experimental and theoretical study, Chem. Mater. 29 (13) (2017) 5617–5628.
[73] H.-S. Qian, S.-H. Yu, J.-Y. Gong, L.-B. Luo, L.-f. Fei, High-quality luminescent tellurium nanowires of several nanometers in diameter and high aspect ratio synthesized by a poly (vinyl pyrrolidone)-assisted hydrothermal process, Langmuir 22 (8) (2006) 3830–3835.
[74] W. Wang, J. Luo, W. Chen, J. Li, W. Xing, S. Chen, Synthesis of mesoporous Fe/N/C oxygen reduction catalysts through NaCl crystallite-confined pyrolysis of polyvinylpyrrolidone, J. Mater. Chem. A 4 (33) (2016) 12768–12773.
[75] K. Niu, B. Yang, J. Cui, J. Jin, X. Fu, Q. Zhao, J. Zhang, Graphene-based non-noble-metal Co/N/C catalyst for oxygen reduction reaction in alkaline solution, J. Power Sources 243 (2013) 65–71.
[76] S.H. Ahn, X. Yu, A. Manthiram, "Wiring" Fe-nx -embedded porous carbon framework onto 1D nanotubes for efficient oxygen reduction reaction in alkaline and acidic media, Adv. Mater. 29 (26) (2017), 1606534.
[77] D. Zhou, L. Yang, L. Yu, J. Kong, X. Yao, W. Liu, Z. Xu, X. Lu, Fe/N/C hollow nanospheres by Fe(iii)-dopamine complexation-assisted one-pot doping as nonprecious-metal electrocatalysts for oxygen reduction, Nanoscale 7 (4) (2015) 1501–1509.
[78] J. Xi, Y. Xia, Y. Xu, J. Xiao, S. Wang, (Fe,Co)@nitrogen-doped graphitic carbon nanocubes derived from polydopamine-encapsulated metal-organic frameworks as a highly stable and selective non-precious oxygen reduction electrocatalyst, Chem. Commun. 51 (52) (2015) 10479–10482.
[79] W. Niu, K. Marcus, L. Zhou, Z. Li, L. Shi, K. Liang, Y. Yang, Enhancing electron transfer and electrocatalytic activity on crystalline carbon-conjugated g-C3N4, ACS Catal. 8 (3) (2018) 1926–1931.
[80] W. Niu, Z. Li, K. Marcus, L. Zhou, Y. Li, R. Ye, K. Liang, Y. Yang, Surface-modified porous carbon nitride composites as highly efficient electrocatalyst for Zn-air batteries, Adv. Energy Mater. 8 (1) (2018), 1701642.
[81] Y. Zheng, J. Liu, J. Liang, M. Jaroniec, S.Z. Qiao, Graphitic carbon nitride materials: controllable synthesis and applications in fuel cells and photocatalysis, Energy Environ. Sci. 5 (5) (2012) 6717–6731.
[82] B. Li, B. Xi, Z. Feng, Y. Lin, J. Liu, J. Feng, Y. Qian, S. Xiong, Hierarchical porous nanosheets constructed by graphene-coated, interconnected TiO2 nanoparticles for ultrafast sodium storage, Adv. Mater. 30 (10) (2018), 1705788.
[83] H. Yu, L. Shang, T. Bian, R. Shi, G.I.N. Waterhouse, Y. Zhao, C. Zhou, L.-Z. Wu, C.-H. Tung, T. Zhang, Nitrogen-doped porous carbon nanosheets templated from g-C3N4 as metal-free electrocatalysts for efficient oxygen reduction reaction, Adv. Mater. 28 (25) (2016) 5080–5086.
[84] Q. Li, D. Xu, J. Guo, X. Ou, F. Yan, Protonated g-C3N4@ polypyrrole derived N-doped porous carbon for supercapacitors and oxygen electrocatalysis, Carbon 124 (2017) 599–610.

[85] J.-J. Lv, Y. Li, S. Wu, H. Fang, L.-L. Li, R.-B. Song, J. Ma, J.-J. Zhu, Oxygen species on nitrogen-doped carbon nanosheets as efficient active sites for multiple electrocatalysis, ACS Appl. Mater. Interfaces 10 (14) (2018) 11678–11688.
[86] R. Wang, T. Yan, L. Han, G. Chen, H. Li, J. Zhang, L.Y. Shi, D. Zhang, Tuning dimensions and structures of nitrogen-doped carbon nanomaterials derived from sacrificial g-C3N4/metal-organic frameworks for enhanced electrocatalytic oxygen reduction, J. Mater. Chem. A 6 (14) (2018) 5752–5761.
[87] D. Gu, F. Wang, K. Yan, R. Ma, J. Wang, A thermally decomposable template route to synthesize nitrogen-doped wrinkled carbon nanosheets as highly efficient and stable electrocatalysts for the oxygen reduction reaction, ACS Sustain. Chem. Eng. 6 (2) (2017) 1951–1960.
[88] Y. Peng, B. Lu, S. Chen, Carbon-supported single atom catalysts for electrochemical energy conversion and storage, Adv. Mater. 30 (2018), 1801995.